

Theory of Auger decay by laser-dressed atoms

Christian Buth* and Kenneth J. Schafer

Department of Physics and Astronomy, Louisiana State University, Baton Rouge, Louisiana 70803, USA

(Dated: August 27, 2009)

We devise an *ab initio* formalism for the quantum dynamics of Auger decay by laser-dressed atoms which are inner-shell ionized by extreme ultraviolet (XUV) light. The optical dressing laser is assumed to be sufficiently weak such that ground-state electrons are neither excited nor ionized by it. However, the laser has a strong effect on continuum electrons which we describe in strong-field approximation with Volkov waves. The XUV light pulse has a low peak intensity and its interaction is treated as a one-photon process. The quantum dynamics of the inner-shell hole creation with subsequent Auger decay is given by equations of motion (EOMs). For this paper, the EOMs are simplified in terms of an essential-states model which is solved analytically and averaged over magnetic subshells. We apply our theory to the $M_{4,5}N_1N_{2,3}$ Auger decay of a $3d$ hole in a krypton atom. The orbitals are approximated by scaled hydrogenic wave functions. A single attosecond pulse produces $3d$ vacancies which Auger decay in the presence of an 800 nm laser with an intensity of $10^{13} \text{ W cm}^{-2}$. We compute the Auger electron spectrum and assess the convergence of the various quantities involved.

PACS numbers: 32.80.Hd, 32.80.Fb, 32.80.Aa, 32.80.Qk

I. INTRODUCTION

The inner-shell ionization of atoms leads to a fascinating array of many-electron effects. Such vacancies decay on an ultrafast time scale by fluorescence or electronic decay. Electronic decay refers to Auger decay [1] and its special variant, Coster-Kronig decay [2]. For low energy transitions in, e.g., light elements or high-lying inner shells in heavier elements, Auger decay is the dominant relaxation process [3, 4]. For deep inner-shell holes, the ion relaxes in terms of cascades of fluorescence and electronic decay processes. All atomic electrons are involved either directly in the photoionization with subsequent electronic or fluorescence decay or indirectly due to a rearrangement of the atomic electrons in the presence of newly formed holes, so-called core relaxation [5]. Furthermore, at photon energies near the ionization threshold, the outgoing photoelectrons are slow and may interact significantly with the ionic remnant. If the subsequent electronic decay process is fast, outgoing photo- and Auger electrons even repel each other appreciably. This phenomenon is dubbed post-collision interaction [5, 6, 7, 8]. Generally, we will refer to electronic decay and Auger decay and will not explicitly distinguish Coster-Kronig decay. They are fundamental processes that are pure manifestations of electron correlations. In this way, electronic decay processes are ideal for an investigation with the methods of attosecond science [9, 10, 11, 12, 13] which aim to measure and control the motion of electrons on their natural time scale, which is the attosecond.

Attosecond light was first used to measure the Auger decay time of $3d$ vacancies (M shell) in

krypton atoms [14, 15]. Such vacancies undergo $M_{4,5}N_1N_{2,3}$ Auger decay which has been studied experimentally in the frequency domain [16, 17, 18, 19]. The time-domain study of Auger decay represents a seminal experiment in several ways. On the one hand, it demonstrates the power of the newly created attosecond methodology by comparing its results with existing data. On the other hand, the study of transient electron motion with attosecond science has so far been restricted to mostly one-electron processes, e.g., Refs. [13, 20, 21] and references therein. However, the most profound goal of attosecond science remains the study of electron correlations.

Clearly, controlling a process on an attosecond time scale requires extreme ultraviolet (XUV) light for its short cycle period. Naturally, XUV light targets inner shells for which the photoabsorption cross section is highest at these wavelengths. The degree of control over inner-shell electron motion is potentially limited compared with valence electrons because of weak present-day attosecond light sources and the fact that postgeneration pulse shaping capabilities in the XUV and x-ray domains are severely limited, e.g., only an amplitude shaping can be accomplished so far with electromagnetically induced transparency for x rays [22]. However, the attosecond light can be augmented by an additional optical laser, a so-called two-color problem. For moderate intensities, the influence of the optical laser on electrons in the atomic ground state and hence the two-electron interaction among them can be neglected, e.g., noble gases can sustain very high electric fields before ionizing. For all elements, the impact of the optical laser on inner-shell electrons is negligible. For the optical laser to impact inner-shell electrons, its intensity needs to be so high that it would valence ionize the atom. Yet it can be used to structure the continuum, i.e., have an influence on liberated electrons, and in that way enable profound control

*Corresponding author; Electronic address: christian.buth@web.de

over electronic processes [13, 22]. A seminal experiment along the above-mentioned lines—but on a much slower (picosecond) time scale—is ultrafast laser control, using coherent excitation with short laser pulses, of the energy and proximity of Rydberg electrons in an atom by Pisharody and Jones [23]. To demonstrate their ability to control electron dynamics, they showed that the autoionization of the doubly-excited barium atoms is due to electron-electron collisions instead of a slow transfer of energy. Another notable work is the theoretical investigation of an XUV pump-probe scheme for the study of the simultaneous two-electron emission in helium by Hu and Collins [24].

The time-domain measurement of the Auger decay of the $3d$ vacancy in krypton atoms [14] has been approached theoretically in two different ways [25, 26, 27]. First, Yakovlev and Scrinzi [25] devised a model to support the experimental study [14]. They made a simple rate equation ansatz to represent the $3d$ hole population. This population was used together with the Auger electron wave function to replace the transition dipole matrix element in a formula to determine the laser-streaked photoelectron spectra of XUV-ionized atoms [28]. Second, Smirnova *et al.* [26] revisited the question of Auger decay by weakly laser-dressed atoms in terms of a fully coherent system of equations of motion (EOMs) formulation for an essential-states model [29] using Hartree products. It is constructed to describe the Auger electron spectrum as simply as possible decoupling the EOMs in terms of a parametric decay width from Weisskopf-Wigner theory [30, 31, 32] and solving the resulting system of equations analytically. Based on the ideas in Refs. [25, 26, 27] Zhao and Lin [33] and Wickenhauser *et al.* [34] studied Fano resonances. Kazansky and Kabachnik [35, 36] developed an *ab initio* theory for the solution of the time-dependent Schrödinger equation for photoionization of inner atomic shells in terms of a Fano-Feshbach formalism with short pulses that takes into account near-threshold effects. Finally, Smirnova *et al.* [37] applied the theory in Ref. [26] to devise a scheme to use electron correlations to make attosecond measurements without attosecond pulses.

Our study goes beyond previous work [25, 26, 27] and overcomes many of its restrictions. We develop a nonrelativistic multideterminantal *ab initio* formalism for the interaction of two-color light with atoms. We set out from the Hartree-Fock-Slater (HFS) approximation for the atomic orbitals. Such mean-field orbitals are typically a good representation to describe Auger decay [6]. Using general spin-singlet configuration-state functions, we derive EOMs. We treat the interaction with light semiclassically because, in contrast to a one-electron quantum electrodynamic formalism [38, 39], band width and pulse duration are treated more easily. Naturally, these play a decisive role in attosecond science. The general EOMs are subsequently simplified to an essential-states model [29] and the equations are solved analytically in this special case considering, in contrast to the work in

Ref. [26], also the laser dressing of the photoelectrons. Furthermore, the laser dressing is, in our case, not required to be weak, yet the intensity should remain below the excitation and ionization threshold of atomic ground-state electrons. We make a model for the atomic electronic structure in terms of scaled hydrogenic wave functions [25, 27]. Our formalism is a basis for the study of more complex situations in Auger decay and its control. In forthcoming papers [40], we will investigate the interference between Auger electrons from a twin XUV attosecond pulse. Further, one can examine what new avenues for the control of Auger processes open up when one relaxes the assumption of an essential-states model to a multichannel treatment.

The paper is structured as follows. In Sec. II, we devise EOMs to treat the quantum dynamics of Auger decay on an *ab initio* level. Volkov waves are introduced in Sec. III to describe the laser dressing. The EOMs are solved analytically for an essential-states model in Sec. IV. We devote Sec. V to the determination of the dipole and two-electron matrix elements for our formalism. We then apply our theory to the laser-dressed Auger decay of krypton $3d$ vacancies; computational details are given in Sec. VI and results are presented in Sec. VII. Conclusions are drawn in Sec. VIII.

Our equations are formulated in atomic units [41]. The Bohr radius $1 \text{ bohr} = 1 a_0$ is the unit of length and $1 t_0$ represents the unit of time. The unit of energy is $1 \text{ hartree} = 1 E_h$. Generally, we use the indices h, i, j, m, \dots to denote occupied orbitals, a, b, c, d, \dots for unoccupied orbitals, and p, q, r, s, \dots for orbitals which may be occupied or unoccupied.

II. QUANTUM DYNAMICS OF PHOTOIONIZATION AND AUGER DECAY

This section forms the core of our theory. In Sec. II A, we describe the schematic of XUV photoionization with subsequent Auger decay. The quantum mechanical foundation is laid out in terms of an *ab initio* description in Secs. II B, II C, and II D, where we introduce the Hamiltonian and the states involved. The full nonrelativistic formalism is simplified using an approximate Hamiltonian in Sec. II E which comprises only those two-electron integrals which are essential for Auger decay. We correct for our omissions by adjusting the energies of the involved states appropriately. Finally, we use the time-dependent Schrödinger equation with the approximate Hamiltonian to formulate EOMs in Sec. II F for the quantum dynamics of XUV absorption and Auger decay.

A. Schematic of the processes

Auger decay can be treated theoretically in various degrees of sophistication [6, 42]. We focus on a description in terms of a single isolated resonance (no decay cas-

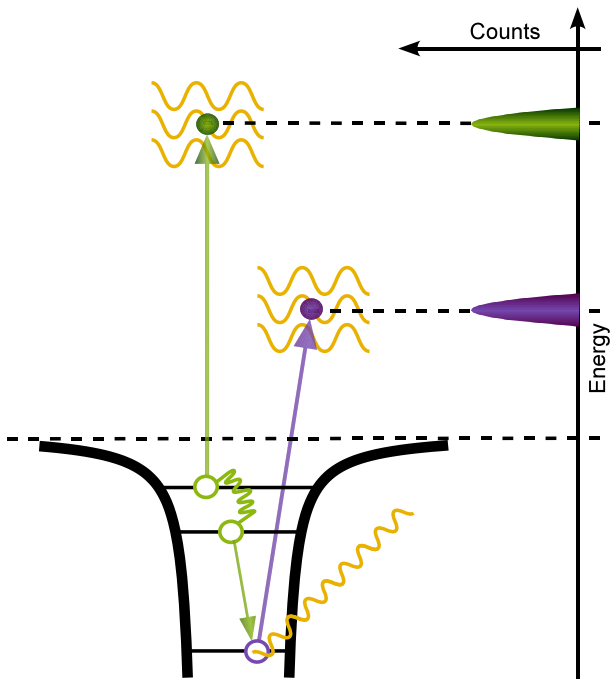


FIG. 1: (Color online) Schematic of laser-dressed XUV photoionization of an inner-shell electron with a subsequent Auger decay. Only participating electrons are drawn. Photoelectron and Auger electron lines are influenced by a dressing laser and are observed in an electron spectrometer. Similar to Fig. 1a in Ref. [14].

cares). In the language of a full scattering process, Auger decay is a resonance in the double photoionization cross section [6, 42]. The scattering of an XUV photon γ off an atom A leads to the formation of a dication A^{++} and the emission of two electrons e_P^- and e_A^- ,

$$A + \gamma \longrightarrow A^{++} + e_P^- + e_A^-. \quad (1)$$

Here, we ignore electron correlations among the ground-state electrons and in the cation and the dication. We also ignore the interaction between the outgoing electrons and the remaining ground-state electrons and the repulsion between the outgoing electrons, so-called post-collision interactions [5, 8].

Assuming intermediate singly-ionized resonance states, we break up Eq. (1) into two separate processes: the photoionization of an atomic inner shell with subsequent Auger decay [6, 42] which is depicted in Fig. 1. To begin with, let us disregard laser dressing. A level scheme of the states participating in the photoionization and subsequent Auger decay are shown in Fig. 2. The atom is initially in the ground state with energy E_0 . Then, it absorbs an XUV photon with an energy of ω_X . This leads to the formation of a singly inner-shell ionized cation with energy E^+ and the ejection of a photoelectron. With the Einstein relation, the peak of the energy distribution of the photoelectron spectrum—the nominal photoelectron energy Ω_P —is found to be $\bar{k}_P^2/2 = \Omega_P =$

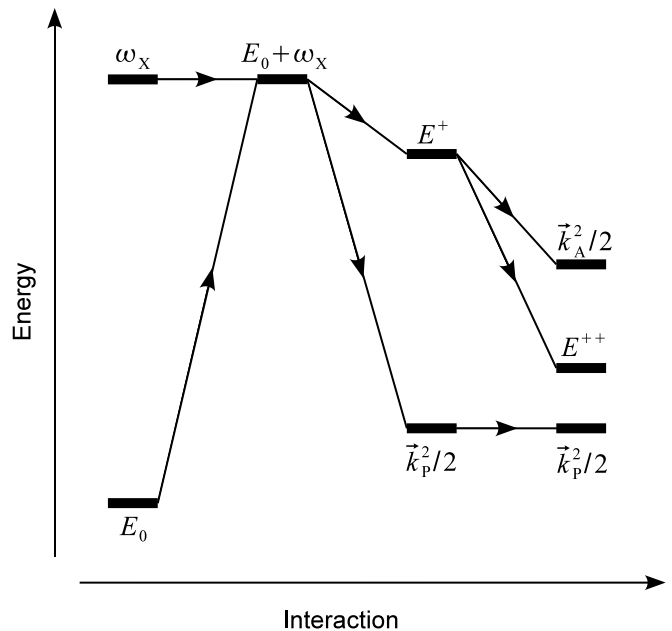


FIG. 2: Energy level scheme of the production of an inner-shell hole by XUV photon absorption and its subsequent Auger decay. The XUV photon energy is ω_X , the atomic ground-state energy is E_0 , the singly-ionized state has an energy E^+ , and the doubly-ionized state energy is E^{++} . The photoelectron has a nominal kinetic energy of $\bar{k}_P^2/2 = \Omega_P$ and the Auger electron of $\bar{k}_A^2/2 = \Omega_A$.

$E_0 + \omega_X - E^+$ [3, 32]. The inner-shell hole Auger decays; it is filled by a valence electron and the excess energy is transferred ultrafast by electron correlations to a second valence electron which is expelled. This gives rise to an Auger line in the electron spectrum at the nominal energy $\bar{k}_A^2/2 = \Omega_A = E^+ - E^{++}$. Afterwards, the system is in a dicationic final state with energy E^{++} . This approximate mechanism of an ionization step with a following electronic decay step is frequently referred to as two-step model of Auger decay [6, 42]. Usually, this is a good approximation for atoms and molecules. However, in condensed matter, rearrangement processes take place which necessitate treating Auger decay as a one-step process [6, 42].

Next, we consider the influence of an optical dressing laser. Its intensity is assumed to be sufficiently low that it does not excite or ionize atomic ground-state electrons. However, the presence of the laser has a strong impact on the outgoing electrons and this has important consequences for the observed signal. We use Volkov waves [43, 44] to describe continuum electrons and we exclude the possibility that the initial XUV absorption does not ionize the atom but induces only an excitation to a Rydberg orbital. This means that effects such as electromagnetically induced transparency for x rays [22, 38, 39, 45, 46, 47] are not represented in our formalism. Always, the laser intensity is assumed

to be sufficiently low as not to modify the Auger decay rate noticeably with respect to the laser-free case. In other words, we neglect the impact of the laser on the energies E_0 , E^+ , and E^{++} and the Auger decay-relevant two-electron matrix elements (three atomic ground-state orbitals and a continuum electron) because they are only weakly perturbed.

B. Atomic electronic structure

We assume a Z -electron atom with a closed-shell spin-singlet ground state. The ground-state wave function is approximated by a Slater determinant of one-electron orbitals $\Phi_0(\vec{r}_1 \sigma_1, \dots, \vec{r}_Z \sigma_Z)$. Electron coordinates are given by \vec{r}_i and spin projection quantum numbers are given by σ_i for $i \in \{1, \dots, Z\}$. We use the formalism of second quantization where $\hat{b}_{p\sigma}$ and $\hat{b}_{p\sigma}^\dagger$ are an annihilator and a creator of an electron in the spin orbital $\psi_{p\sigma}(\vec{r})$, respectively, which is the tensor product of a spatial orbital $\varphi_p(\vec{r})$ and a spinor of projection quantum number σ [41]. We define spin up $\sigma = \frac{1}{2} = \uparrow$ and spin down $\sigma = -\frac{1}{2} = \downarrow$ and make the following ansatz for the atomic ground state,

$$|\Phi_0\rangle = \prod_{i=1}^{Z/2} \hat{b}_{i\uparrow}^\dagger \hat{b}_{i\downarrow}^\dagger |0\rangle, \quad (2)$$

using the vacuum state $|0\rangle$ [41].

Let the full atomic electronic structure Hamiltonian be denoted by \hat{H}_{AT} . It consists of the kinetic energy of the electrons, the electron-nucleus attraction, and the electron-electron repulsion [41]. We determine atomic orbitals within the HFS approximation [48, 49] to \hat{H}_{AT} . In a next step, we use the HFS orbitals to represent \hat{H}_{AT} . As the HFS approximation is typically good, \hat{H}_{AT} naturally decomposes into a part which is large and another which can be treated as a perturbation. We can rewrite \hat{H}_{AT} as follows:

$$\hat{H}_{\text{AT}} = \hat{H}_{\text{HFS}} + \hat{H}_{\text{CH}} + \hat{H}_{\text{ee}}, \quad (3)$$

assuming a representation in terms of the atomic orbitals. We discuss these terms in the following paragraphs [41].

The HFS Hamiltonian in Eq. (3) represented in terms of HFS orbitals reads

$$\hat{H}_{\text{HFS}} = \sum_p \varepsilon_p [\hat{b}_{p\uparrow}^\dagger \hat{b}_{p\uparrow} + \hat{b}_{p\downarrow}^\dagger \hat{b}_{p\downarrow}], \quad (4)$$

with the spin-independent orbital energies ε_p . For notational clarity, we assume a countably infinite set of final states in Eq. (4) and in this entire section, i.e., we assume a finite volume for box normalization of continuum wave functions [32] or a (finite-element) basis set expansion of the radial part of the atomic orbitals times spherical harmonics [38]. From Sec. IV D onward, we will use continuum wave functions, namely, plane waves and Volkov waves [32, 43, 44].

The contribution \hat{H}_{CH} in Eq. (3) allows for the fact that in the Hartree-Fock-Slater approximation (4) the electron-nuclear interaction and the electron-electron interaction are replaced by the one-electron central potential $V_{\text{HFS}}(r)$ where the nucleus is at the origin of a spherical polar coordinate system and the electron is at radius r [38]. This replacement is reversed by the corrective term

$$\hat{H}_{\text{CH}} = \sum_{p,q} \langle \varphi_p | \hat{h}_{\text{CH}} | \varphi_q \rangle [\hat{b}_{p\uparrow}^\dagger \hat{b}_{q\uparrow} + \hat{b}_{p\downarrow}^\dagger \hat{b}_{q\downarrow}]. \quad (5)$$

with

$$\hat{h}_{\text{CH}} = -V_{\text{HFS}}(r) - \frac{Z}{r} \quad (6)$$

in addition to the explicit treatment of electron correlations in the next paragraph. There are no mixed terms involving a spin-up and a spin-down orbital in Eq. (5) because the interaction (6) does not depend on the spin.

Electron correlations in Eq. (3) are described by

$$\hat{H}_{\text{ee}} = \frac{1}{2} \sum_{\sigma, \sigma', \xi, \xi' = \downarrow}^{\uparrow} \sum_{p, p', q, q'} V_{p\sigma p'\sigma' q\xi q'\xi'} \hat{b}_{p\sigma}^\dagger \hat{b}_{p'\sigma'}^\dagger \hat{b}_{q'\xi'} \hat{b}_{q\xi}. \quad (7)$$

which is the only two-particle operator [32, 41] in the total Hamiltonian of the atom. The two-electron integrals in Eq. (7) are defined in terms of HFS spin orbitals by $V_{p\sigma p'\sigma' q\xi q'\xi'} = \langle \psi_{p\sigma} \psi_{p'\sigma'} | \hat{h}_{\text{ee}} | \psi_{q\xi} \psi_{q'\xi'} \rangle$. The Coulomb interaction is

$$\hat{h}_{\text{ee}} = \frac{1}{|\vec{r} - \vec{r}'|}, \quad (8)$$

where \vec{r} and \vec{r}' represent the coordinates of two electrons in the atom.

C. Atom in xuv light

We assume that the XUV light is linearly polarized along the direction \vec{e}_X and the wavelength is sufficiently large for the electric dipole approximation to be adequate [50]. Then, the Hamiltonian for the interaction of electrons with XUV light [50] reads

$$\hat{H}_X = \sum_{p,q} D_{pq}(t) [\hat{b}_{p\uparrow}^\dagger \hat{b}_{q\uparrow} + \hat{b}_{p\downarrow}^\dagger \hat{b}_{q\downarrow}], \quad (9)$$

using the matrix element $D_{pq}(t) \equiv \langle \varphi_p | \hat{h}_X | \varphi_q \rangle$ in terms of atomic orbitals of the spin-independent one-electron interaction with XUV light in length form,

$$\hat{h}_X = \vec{r} \cdot \vec{E}_X(t). \quad (10)$$

We use for the electric field of the XUV light

$$\vec{E}_X(t) = \varepsilon_X(t) \vec{e}_X \cos(\omega_X t), \quad (11)$$

with the pulse envelope $\varepsilon_X(t)$ and the angular frequency ω_X . With Eqs. (10) and (11), we can rewrite the light-electron interaction as follows:

$$D_{pq}(t) = d_{pq} \frac{\varepsilon_X(t)}{2} [e^{i\omega_X t} + e^{-i\omega_X t}], \quad (12)$$

where the atomic dipole matrix elements are given by $d_{pq} \equiv \langle \varphi_p | \vec{r} \cdot \vec{e}_X | \varphi_q \rangle$.

The complete Hamiltonian consists of the atomic electronic structure (3) and the interaction with the XUV light (9) and reads

$$\hat{H} = \hat{H}_{\text{AT}} + \hat{H}_X. \quad (13)$$

It will serve as the basis to treat the quantum dynamics of XUV absorption and subsequent Auger decay.

D. Excited states

Having formulated the Hamiltonian of the problem (13) and having specified the ground state (2), we need to incorporate singly- and doubly- excited states in our description to represent photoabsorption and Auger decay. We use a single configuration-state function (CSF), which is a linear combination of singly- and doubly-excited determinants, to stand for a singly- and a doubly-excited state, respectively. Generally, singly-excited determinants are a satisfactory approximation to singly-excited wave functions which is the reason for the success of Koopmans' theorem [41]. However, doubly-excited states are not so well represented by doubly-excited determinants because of hole-hole repulsion effects and continuum electron interaction. To overcome this approximation, one needs to allow for configuration interaction [41].

Spin-singlet singly-excited states are represented by [32, 41]

$$|^1\Phi_h^a\rangle = \frac{1}{\sqrt{2}} [\hat{b}_{a\uparrow}^\dagger \hat{b}_{h\uparrow} + \hat{b}_{a\downarrow}^\dagger \hat{b}_{h\downarrow}] |\Phi_0\rangle = \frac{1}{\sqrt{2}} [|\Phi_h^a\rangle + |\Phi_h^{\bar{a}}\rangle]. \quad (14)$$

Here, $\hat{b}_{h\sigma}$ creates a hole in the orbital h with spin projection number σ by destroying the electron and $\hat{b}_{a\sigma}^\dagger$ creates an electron in the orbital a with spin projection number σ . The hole orbital indices h which are taken into account form the set \mathcal{H} ; the indices for virtual (unoccupied) orbitals are $a > \frac{Z}{2}$ (Z is even because we consider only closed-shell atoms). After the second equals sign in Eq. (14), we introduce a concise determinantal notation [41]. The bar over spatial orbital indices indicates a spin orbital with spin down; no bar refers to a spin orbital with spin up.

There are five classes of doubly-excited spin-singlet configuration-state functions (Table 2.7 in Ref. [41]). We focus on the two classes in which all four spatial orbitals are distinct. Using the concise notation of Eq. (14), we

have

$$|{}^1_A\Phi_{ij}^{ab}\rangle = \frac{1}{\sqrt{12}} [2|\Phi_{ij}^{ab}\rangle + 2|\Phi_{ij}^{\bar{a}\bar{b}}\rangle - |\Phi_{ij}^{\bar{b}a}\rangle + |\Phi_{ij}^{\bar{a}b}\rangle + |\Phi_{ij}^{\bar{a}\bar{b}}\rangle - |\Phi_{ij}^{b\bar{a}}\rangle], \quad (15a)$$

$$|{}^1_B\Phi_{ij}^{ab}\rangle = \frac{1}{2} [|\Phi_{ij}^{\bar{b}a}\rangle + |\Phi_{ij}^{\bar{a}b}\rangle + |\Phi_{ij}^{\bar{a}\bar{b}}\rangle + |\Phi_{ij}^{b\bar{a}}\rangle]. \quad (15b)$$

The pairs of orbital indices (i, j) of double vacancies with $i < j$, which are considered, constitute the set \mathcal{F} . With the restrictions $a < b$ and $a, b > \frac{Z}{2}$ for the virtual orbital indices, we enumerate all distinct doubly-excited configurations.

The energy of the ground state (2) is found with the electronic Hamiltonian (3) as follows:

$$E_0 = \langle \Phi_0 | \hat{H}_{\text{AT}} | \Phi_0 \rangle = 2 \sum_{i=1}^{Z/2} \varepsilon_i + \langle \Phi_0 | \hat{H}_{\text{CH}} + \hat{H}_{\text{ee}} | \Phi_0 \rangle. \quad (16)$$

The first term on the right-hand side is twice the sum of occupied Hartree-Fock-Slater orbital energies dubbed \mathcal{E}_0 [41]. The singly-excited states (14) have an energy of

$$E_h^a = \langle {}^1\Phi_h^a | \hat{H}_{\text{AT}} | {}^1\Phi_h^a \rangle = \mathcal{E}_0 - \varepsilon_h + \varepsilon_a + \langle {}^1\Phi_h^a | \hat{H}_{\text{CH}} + \hat{H}_{\text{ee}} | {}^1\Phi_h^a \rangle, \quad (17)$$

and the doubly-excited states (15) have an energy of

$$\begin{aligned} E_{ij}^{ab} &\equiv E_{ij,A}^{ab} = E_{ij,B}^{ab} = \langle {}^1_A\Phi_{ij}^{ab} | \hat{H}_{\text{AT}} | {}^1_A\Phi_{ij}^{ab} \rangle \\ &= \mathcal{E}_0 - \varepsilon_i - \varepsilon_j + \varepsilon_a + \varepsilon_b + \langle {}^1_A\Phi_{ij}^{ab} | \hat{H}_{\text{CH}} + \hat{H}_{\text{ee}} | {}^1_A\Phi_{ij}^{ab} \rangle. \end{aligned} \quad (18)$$

We have $E_{ij,A}^{ab} = E_{ij,B}^{ab}$ because both doubly-excited CSFs consist of determinants with excitations from the same spatial orbitals into the same spatial orbitals, only the spinors change. As our nonrelativistic Hamiltonian (3) does not depend on spin, especially, it does not contain spin-orbit coupling, the energies are the same for all the excited determinants and thus also for the configuration-state functions A and B.

E. Simplified Hamiltonian

We have formulated a full *ab initio* description of the problem with a truncated excitation manifold [41]. Our framework represents an ideal starting point for further simplifications. Eventually, it will be reduced to an essential-states model in Sec. IV that contains only the absolutely necessary energies and matrix elements to still describe the physics of the processes. We form a matrix representation of the Hamiltonian \hat{H} [Eq. (13)] in terms of the orthonormal basis,

$$\mathcal{B} = \{ |\Phi_0\rangle, |{}^1\Phi_h^a\rangle, |{}^1_\gamma\Phi_{ij}^{ab}\rangle \mid h \in \mathcal{H}, (i, j) \in \mathcal{F}, a, b > Z/2, a < b, \gamma \in \{A, B\} \}. \quad (19)$$

We decompose the representation of \hat{H} into an exactly solvable part \hat{H}_0 , given by the diagonal elements of \hat{H} ,

and a perturbation \hat{H}_1 , given by the off-diagonal elements of \hat{H} . This is a so-called Epstein-Nesbet partitioning [51, 52, 53]. The exactly solvable diagonal part is written compactly in first quantization as

$$\begin{aligned} \hat{H}_0 = & |\Phi_0\rangle E_0 \langle \Phi_0| + \sum_{h \in \mathcal{H}} \sum_{a > Z/2} |^1\Phi_h^a\rangle E_h^a \langle ^1\Phi_h^a| \\ & + \sum_{(i,j) \in \mathcal{F}} \sum_{\substack{a,b > Z/2 \\ a < b}} \sum_{\gamma \in \{A,B\}} |^1\Phi_{ij}^{ab}\rangle E_{ij,\gamma}^{ab} \langle ^1\Phi_{ij}^{ab}|, \end{aligned} \quad (20)$$

where we use the energies from Eqs. (16), (17), and (18). These energies are well suited to be treated as (experimental) parameters [see Sec. VI]. Here, \hat{H}_X makes no contribution to the diagonal matrix elements of \hat{H} because it consists only of off-diagonal elements.

The perturbation is given by \hat{H}_1 . We do not use all off-diagonal elements of \hat{H} for \hat{H}_1 and, additionally, we make approximations to the ones we retain. We use

$$\begin{aligned} \hat{H}_1 = & \sum_{h \in \mathcal{H}} \sum_{a > Z/2} [|\Phi_0\rangle \langle \Phi_0| \hat{H}_X |^1\Phi_h^a\rangle \langle ^1\Phi_h^a| \\ & + |^1\Phi_h^a\rangle \langle ^1\Phi_h^a| \hat{H}_X | \Phi_0\rangle \langle \Phi_0|] \\ & + \sum_{\substack{(i,j) \in \mathcal{F} \\ h \in \mathcal{H}}} \sum_{\substack{a,b > Z/2 \\ a < b}} \sum_{\gamma \in \{A,B\}} [|^1\Phi_h^a\rangle \langle ^1\Phi_h^a| \hat{H}_{ee} |^1\Phi_{ij}^{ab}\rangle \langle ^1\Phi_{ij}^{ab}| \\ & + |^1\Phi_{ij}^{ab}\rangle \langle ^1\Phi_{ij}^{ab}| \hat{H}_{ee} |^1\Phi_h^a\rangle \langle ^1\Phi_h^a|]. \end{aligned} \quad (21)$$

Here, \hat{H}_{HFS} [Eq. (4)] makes no contribution because it consists only of diagonal elements. The impact of \hat{H}_{CH} [Eq. (5)] is neglected totally and we consider the energies in Eq. (20) to be parameters which shall compensate for this and the other omissions that influence the energies of the involved states. Similarly, electron correlations \hat{H}_{ee} are only included when they cause transitions between singly- and doubly-excited states, i.e., they are taken into account when they are responsible for Auger decay which cannot be understood in a mean-field picture. In principle, the neglected matrix elements can be incorporated allowing one to carry out a full *ab initio* treatment of the problem.

F. Equation of motion formulation of photoionization and Auger decay

To describe a photoionization process with subsequent Auger decay, we solve the time-dependent Schrödinger equation

$$\hat{H} |\Psi, t\rangle = i \frac{\partial}{\partial t} |\Psi, t\rangle \quad (22)$$

for an atom in XUV light. In terms of the states in the basis \mathcal{B} [Eq. (19)], a general state ket (or wave packet) is given by

$$\begin{aligned} |\Psi, t\rangle = & c_0(t) e^{-iE_0 t} |\Phi_0\rangle + \sum_{\substack{h \in \mathcal{H} \\ a > Z/2}} c_h^a(t) e^{-iE_h^a t} |^1\Phi_h^a\rangle \\ & + \sum_{\substack{(i,j) \in \mathcal{F} \\ \gamma \in \{A,B\}}} \sum_{\substack{a,b > Z/2 \\ a < b}} c_{ij,\gamma}^{ab}(t) e^{-iE_{ij,\gamma}^{ab} t} |^1\Phi_{ij}^{ab}\rangle, \end{aligned} \quad (23)$$

which we insert into the time-dependent Schrödinger equation (22). Exploiting $\hat{H}_0 |\phi\rangle = E_\phi |\phi\rangle$ for states $|\phi\rangle \in \mathcal{B}$ with energies E_ϕ , we arrive at the EOMs for the expansion coefficients $c_0(t)$, $c_h^a(t)$, and $c_{ij,\gamma}^{ab}(t)$ by projecting on $\langle \phi|$ for all $|\phi\rangle \in \mathcal{B}$. The atom is initially in the ground state which implies the initial conditions $c_0(0) = 1$ and $c_h^a(0) = c_{ij,\gamma}^{ab}(0) = 0$.

We get the first EOM for $\langle \phi| = \langle \Phi_0|$ which represents the rate of change of the ground-state amplitude,

$$\dot{c}_0(t) = -i\sqrt{2} \sum_{h \in \mathcal{H}} \sum_{a > Z/2} D_{ha}(t) e^{i(E_0 - E_h^a)t} c_h^a(t). \quad (24)$$

We consider here the weak absorption limit, i.e., $c_0(t) \approx 1$ for all times. The rate of change will, nevertheless, prove highly beneficial in determining the cross section in Sec. IV E and the photoelectron spectrum in Sec. IV F.

The second EOM results from $|\phi\rangle = |^1\Phi_h^a\rangle$ and describes the inner-shell hole amplitude for $h \in \mathcal{H}$,

$$\begin{aligned} \dot{c}_h^a(t) = & -i\sqrt{2} D_{ah}(t) e^{i(E_h^a - E_0)t} \\ & - i \sum_{(i,j) \in \mathcal{F}} \sum_{\substack{b > Z/2 \\ a \neq b}} \left[-\sqrt{\frac{3}{2}} v_{hb}^* [ij] e^{i(E_h^a - E_{ij,A}^{ab})t} c_{ij,A}^{ab}(t) \right. \\ & \left. - \frac{1}{\sqrt{2}} v_{hb}^* [ij] e^{i(E_h^a - E_{ij,B}^{ab})t} c_{ij,B}^{ab}(t) \right]. \end{aligned} \quad (25)$$

The first term on the right-hand side of the equation represents hole production due to absorption of XUV light; the second term describes the loss of hole amplitude caused by Auger decay. In this equation, the two-electron matrix element in terms of spatial (e.g., Hartree-Fock-Slater) atomic orbitals is denoted by

$$v_{pp'qq'} = \langle \varphi_p \varphi_{p'} | \hat{h}_{ee} | \varphi_q \varphi_{q'} \rangle. \quad (26)$$

Further, we define the antisymmetrized two-electron matrix element $v_{pp'[qq']} = v_{pp'qq'} - v_{pp'q'q}$ and the symmetrized two-electron matrix element $v_{pp'\{qq'\}} = v_{pp'qq'} + v_{pp'q'q}$ which consist of a direct matrix element $v_{pp'qq'}$ and an exchange matrix element $v_{pp'q'q}$.

The third EOM is obtained setting $\langle \phi| = \langle ^1\Phi_{ij}^{ab}|$; it describes the Auger decay amplitude

$$\dot{c}_{ij,A}^{ab}(t) = i\sqrt{\frac{3}{2}} \sum_{h \in \mathcal{H}} v_{hb} [ij] e^{i(E_{ij,A}^{ab} - E_h^a)t} c_h^a(t), \quad (27a)$$

$$\dot{c}_{ij,B}^{ab}(t) = i\frac{1}{\sqrt{2}} \sum_{h \in \mathcal{H}} v_{hb} [ij] e^{i(E_{ij,B}^{ab} - E_h^a)t} c_h^a(t). \quad (27b)$$

We can reduce the EOMs (25) and (27) further by ignoring the electron exchange matrix element v_{hbji} and exploiting the fact that the energies of the doubly-excited states (18) are the same, $E_{ij}^{ab} \equiv E_{ij,A}^{ab} = E_{ij,B}^{ab}$. Then, the second EOM (25) for the inner-shell hole amplitude simplifies to

$$\begin{aligned} \dot{c}_h^a(t) = & -i\sqrt{2} D_{ah}(t) e^{i(E_h^a - E_0)t} \\ & + i2\sqrt{2} \sum_{(i,j) \in \mathcal{F}} \sum_{\substack{b > Z/2 \\ a \neq b}} v_{hbij}^* e^{i(E_h^a - E_{ij}^{ab})t} c_{ij}^{ab}(t), \end{aligned} \quad (28)$$

for $h \in \mathcal{H}$ with the definition $c_{ij}^{ab}(t) \equiv c_{ij,B}^{ab}(t)$. Again ignoring electron exchange and using E_{ij}^{ab} , leads us to the relation $c_{ij,A}^{ab}(t) = \sqrt{3} c_{ij,B}^{ab}(t)$ between Eqs. (27a) and (27b); thereby, we use that both $c_{ij,A}^{ab}(t)$ and $c_{ij,B}^{ab}(t)$ vanish initially. Then, we need to retain only the simplified Eq. (27b) of the two EOMs for the Auger decay amplitude (27) yielding

$$\dot{c}_{ij}^{ab}(t) = i \frac{1}{\sqrt{2}} \sum_{h \in \mathcal{H}} v_{hbi,j} e^{i(E_{ij}^{ab} - E_h^a)t} c_h^a(t). \quad (29)$$

Equations (28) and (29) constitute a linear system of differential equations which contains all phase information and thus describes interference effects.

III. LASER DRESSING

In Sec. II, we devised a formalism to describe the quantum dynamics of the photoionization of the inner shell of an atom by XUV light and the subsequent Auger decay. Here we expand our formalism to include an additional optical dressing laser of moderate intensity. The impact of the laser on ground-state electrons is neglected and only the modification of the continuum wave functions of the photo- and the Auger electron is considered.

To begin with, we simplify the manifold of virtual states by replacing it by free-electron wave functions, the momentum normalized plane waves [32],

$$\varphi_{P,\vec{k}}(\vec{r}, t) = \frac{1}{(2\pi)^{3/2}} e^{i(\vec{k}\cdot\vec{r} - \frac{\vec{k}^2}{2}t)}. \quad (30)$$

This substitution explicitly excludes Rydberg states. It is justified by the fact that we are only concerned with continuum electrons of sizable kinetic energy. A consequence of our replacement is that the new continuum wave functions are no longer strictly orthogonal to the bound-state wave functions because both sorts of wave functions stem from different Hamiltonians: $\frac{\vec{p}^2}{2} = -\frac{\nabla^2}{2}$ and \hat{H}_{HFS} [Eq. (4)] [32]. Note that we exploited strict orthogonality in the derivations of Sec. II.

When we additionally consider a laser field, our replacement of continuum wave functions becomes known as strong-field approximation [44] in which the influence of the Coulomb potential on continuum states is neglected. In other words, laser dressing can be incorporated easily into our treatment by replacing the laser-free continuum functions $\varphi_{P,\vec{k}}(\vec{r}, t)$ by Volkov waves [43, 44] [see Eq. (34) below]. In doing so, electrons in the atomic ground-state orbitals, however, are considered to be uninfluenced by the laser.

The laser pulse is assumed to be long with respect to all other time scales in this paper and is taken to be monochromatic and continuous wave. Let the laser radiation of angular frequency ω_L be linearly polarized with the polarization vector \vec{e}_L . The vector potential is

$$\vec{A}_L(t) = \vec{A}_{L,0} \sin(\omega_L(t + \Delta t)), \quad (31)$$

where the amplitude is $\vec{A}_{L,0} = -\mathcal{A}_L \vec{e}_L$. The laser phase at $t = 0$ can be specified using Δt . Then, the laser electric field follows from

$$\vec{E}_L(t) = -\frac{d\vec{A}_L(t)}{dt} = \vec{E}_{L,0} \cos(\omega_L(t + \Delta t)), \quad (32)$$

where the electric-field amplitude is $\vec{E}_{L,0} = \omega_L \mathcal{A}_L \vec{e}_L$ [see Eq. (11)]. We assume free fields, i.e., a vanishing scalar potential, and the Coulomb gauge [44, 50].

The Hamiltonian of a free electron in a laser field in velocity form [44, 50] is

$$\hat{h}_V = \frac{(\hat{p} + \vec{A}_L(t))^2}{2}, \quad (33)$$

using the electron momentum operator $\hat{p} = -i\vec{\nabla}$. The solution of the time-dependent Schrödinger equation (22) with Hamiltonian (33) reads

$$\varphi_{V,\vec{k}}(\vec{r}, t) = \frac{1}{(2\pi)^{3/2}} e^{i(\vec{k}\cdot\vec{r} - \Phi_V(\vec{k}, t))} \quad (34)$$

and is called a Volkov wave [43, 44, 54]. The Volkov phase is given by

$$\Phi_V(\vec{k}, t) = \frac{1}{2} \int_{-\infty}^t [\vec{k} + \vec{A}_L(t')]^2 e^{\eta t'} dt'. \quad (35)$$

The factor $e^{\eta t'}$ for $\eta > 0$ ensures the convergence of the integral. After the integral has been performed, the limit $\eta \rightarrow 0^+$ is taken. The Volkov phase vanishes at $-\infty$. Inserting Eq. (31) into Eq. (35), we find

$$\begin{aligned} \Phi_V(\vec{k}, t) &= \left(\frac{\vec{k}^2}{2} + U_P \right) t - \vec{k} \cdot \vec{\alpha}_L \cos(\omega_L(t + \Delta t)) \\ &\quad - \frac{U_P}{2\omega_L} \sin(2\omega_L(t + \Delta t)), \end{aligned} \quad (36)$$

where the ponderomotive potential is

$$U_P = \frac{\mathcal{A}_L^2}{4} = \frac{2\pi}{\omega_L^2} \alpha I_{L,0}, \quad (37)$$

with the electric-field amplitude $|\vec{E}_{L,0}| = \sqrt{8\pi \alpha I_{L,0}}$ for a laser with intensity $I_{L,0}$. The fine-structure constant is α . During a laser cycle, the maximum classical excursion from the origin of a free electron is given by [44]

$$\vec{\alpha}_L = \frac{\vec{A}_{L,0}}{\omega_L} = -\frac{\sqrt{8\pi \alpha I_{L,0}}}{\omega_L^2} \vec{e}_L. \quad (38)$$

The exponential of the Volkov phase (36), $e^{-i\Phi_V(\vec{k}, t)}$, can be expanded using the generating function of the generalized Bessel functions $J_m(u, v)$ [44, 55] which reads

$$e^{-i(u \cos \theta + v \sin(2\theta))} = \sum_{m=-\infty}^{\infty} (-i)^m e^{im\theta} J_m(u, v), \quad (39)$$

by setting $\phi = \theta - \frac{\pi}{2}$ in Eq. (10) in Ref. [44]. The $J_m(u, v)$ can be evaluated in terms of the ordinary Bessel functions $J_{m-2n}(u)$ and $J_n(v)$ using [44, 55]

$$J_m(u, v) = \sum_{n=-\infty}^{\infty} J_{m-2n}(u) J_n(v). \quad (40)$$

Another connection to ordinary Bessel functions represents the relation $J_m(u) = J_m(u, 0)$ with which Eq. (39) reduces to the familiar Jacobi-Anger expansion [56]. Finally, the temporal phase factor reduces to

$$e^{-i\Phi_V(\vec{k}, t)} = e^{-i(\frac{k^2}{2} + U_P)t} \sum_{m=-\infty}^{\infty} e^{-im(\omega_L(t+\Delta t) - \frac{\pi}{2})} \times J_m(\vec{\alpha}_L \cdot \vec{k}, \frac{U_P}{2\omega_L}). \quad (41)$$

IV. ESSENTIAL-STATES MODEL FOR LASER-DRESSED PHOTOIONIZATION AND AUGER DECAY

This section is devoted to a solution of the EOMs from Sec. II F for an essential-states model [26, 27, 29] which is a fairly drastic approximation to the model Hamiltonian of Sec. II E. However, it retains the essential physics of the problem. Namely, we include only the states from three magnetic subshells of the occupied orbital manifold and form essential states from them by averaging the dipole and two-electron matrix elements in Sec. IV A over the subshells. Subsequently, we decouple the system of EOMs in Sec. IV B using perturbation theory. The resulting equations are adapted to account for laser dressing following Sec. III and are solved analytically. We obtain the hole-state amplitude in Sec. IV C which is used to find the Auger electron spectrum in Sec. IV D. Finally, we derive the XUV absorption cross section in Sec. IV E and the photoelectron spectrum in Sec. IV F.

A. Matrix elements and energies

To begin with, let us simplify the problem and the notation. We represent photo- and Auger electrons by plane waves (30) with momentum vectors \vec{k}_P and \vec{k}_A , respectively (laser dressing is not treated at this point). Moreover, we make the following replacements: $a \rightarrow \vec{k}_P$ and $b \rightarrow \vec{k}_A$ in our previous equations. Summations over a and b become integrals over \vec{k}_P and \vec{k}_A . As h , i , and j refer to individual orbitals, their use is not meaningful anymore in our model context and are eliminated or adequately substituted as detailed in the following.

To construct the matrix elements of the essential-states model, we note that the set of hole orbital indices \mathcal{H} refers to orbitals from a single magnetic subshell. The pairs $(i, j) \in \mathcal{F}$ refer to orbital i from one magnetic subshell and orbital j from another magnetic subshell. The number of single hole states is $\#\mathcal{H}$ and the number of

double hole states is $\#\mathcal{F}$. The XUV interaction matrix element is taken to be

$$\bar{d}(\vec{k}_P) = Q_d \sqrt{\frac{1}{\#\mathcal{H}} \sum_{h \in \mathcal{H}} |d_{\vec{k}_P h}|^2} \quad (42)$$

while the Auger decay matrix element is

$$\bar{v}(\vec{k}_A) = Q_v \sqrt{\frac{1}{\#\mathcal{H} \#\mathcal{F}} \sum_{h \in \mathcal{H}} \sum_{(i,j) \in \mathcal{F}} |v_{h \vec{k}_A ij}|^2}. \quad (43)$$

Here, $Q_d > 0$ is the strength of the dipole matrix element and $Q_v > 0$ is the strength of the two-electron matrix element. Both strengths will be determined later in Eqs. (70) and (54), respectively, based on (experimental) parameters. We chose to use the rms value to form average matrix elements because in the following equations frequently the modulus squared of the matrix elements is used.

Within the scope of our essential-states model, the energies of the states of Sec. II D and Fig. 2 are as follows. The ground-state energy (16) is $E_0 = \mathcal{E}_0$, neglecting the influence of $\hat{H}_{CH} + \hat{H}_{ee}$. The energy of singly-excited states (17) is decomposed into the kinetic energy of the photoelectron $\frac{\vec{k}_P^2}{2}$ and the energy of the cation E^+ . It becomes $E_h^a \rightarrow \frac{\vec{k}_P^2}{2} + E^+$ with $E^+ = \mathcal{E}_0 - \varepsilon_h$ (the orbital indices in \mathcal{H} denote orbitals from the same subshell and thus ε_h is the same for all $h \in \mathcal{H}$). For doubly-excited states (18), we set $E_{ij}^{ab} \rightarrow \frac{\vec{k}_P^2 + \vec{k}_A^2}{2} + E^{++}$ with $E^{++} = \mathcal{E}_0 - \varepsilon_i - \varepsilon_j$ being the energy of the dication [again ε_i and ε_j are the same for all $(i, j) \in \mathcal{F}$]. With these definitions, we find for the single ionization potential $I^+ = E^+ - E_0 = -\varepsilon_h$ and for the double ionization potential $I^{++} = E^{++} - E_0 = -\varepsilon_i - \varepsilon_j$ [see also Fig. 2]. The nominal photoelectron energy from the stationary-state energy level scheme is $\Omega_P = E_0 - E^+ + \omega_X$. Likewise, $\Omega_A = E^+ - E^{++}$ is the nominal Auger electron energy.

Under these assumptions, we find for the inner-shell hole amplitude (28)—in which we replaced the hole index h , by the subscript P and the double index ij by the subscript A—the expression

$$\begin{aligned} \dot{c}_{\vec{k}_P}^{\vec{k}_P}(t) &= \frac{-i}{\sqrt{2}} \bar{d}(\vec{k}_P) \varepsilon_X(t) e^{i(\frac{\vec{k}_P^2}{2} - \Omega_P)t} \\ &+ i2\sqrt{2} \underbrace{\int_{\mathbb{R}^3} \bar{v}^*(\vec{k}_A) e^{-i(\frac{\vec{k}_A^2}{2} - \Omega_A)t} \bar{c}_{\vec{k}_P \vec{k}_A}^{\vec{k}_P}(t) d^3k_A}_{\equiv w(\vec{k}_P, t)}. \end{aligned} \quad (44)$$

The Auger decay amplitude (29) is

$$\dot{c}_{\vec{k}_P \vec{k}_A}^{\vec{k}_P \vec{k}_A}(t) = \frac{i}{\sqrt{2}} \bar{v}(\vec{k}_A) e^{i(\frac{\vec{k}_A^2}{2} - \Omega_A)t} \bar{c}_{\vec{k}_P}^{\vec{k}_P}(t). \quad (45)$$

The EOMs of the essential-states model are formed by Eqs. (44) and (45). They are very similar to Eqs. (10) and (11) in Ref. [26, 57].

B. Perturbative decoupling

Despite our considerable simplifications in Sec. IV A, Eqs. (44) and (45) still form a linear system of coupled integrodifferential equations. The coupling stems from the second term $w(\vec{k}_P, t)$ on the right-hand side of Eq. (44). It describes the Auger decay of inner-shell holes and can be approximated in terms of second-order time-dependent perturbation theory (Weisskopf-Wigner theory) [30, 31, 32]. This treatment allows us to decouple the differential equation (44) by eliminating the dependence on $\bar{c}_A^{\vec{k}_P \vec{k}_A}(t)$ in terms of a decay width Γ and an energy shift Δ_R as follows:

$$w(\vec{k}_P, t) = \left(-i\Delta_R - \frac{\Gamma}{2}\right) \bar{c}_P^{\vec{k}_P}(t). \quad (46)$$

The energy shift of the resonance state follows from

$$\begin{aligned} \Delta_{R,h} &= \sum_{(i,j) \in \mathcal{F}} \sum_{\gamma \in \{A,B\}} \text{Pr} \int_{\mathbb{R}^3} \frac{|\langle \gamma^1 \Phi_{ij}^{\vec{k}_P \vec{k}_A} | \hat{H}_1 | \gamma^1 \Phi_h^{\vec{k}_P} \rangle|^2}{E_h^{\vec{k}_P} - E_{ij,\gamma}^{\vec{k}_P \vec{k}_A}} d^3 k_A \\ &\approx \sum_{(i,j) \in \mathcal{F}} \text{Pr} \int_{\mathbb{R}^3} \frac{2|v_h \bar{k}_A ij|^2}{E_h^{\vec{k}_P} - E_{ij}^{\vec{k}_P \vec{k}_A}} d^3 k_A, \end{aligned} \quad (47)$$

where Pr indicates that the principle value of the integral has to be taken. The result was obtained by neglecting electron exchange and using $E_{ij}^{\vec{k}_P \vec{k}_A} \equiv E_{ij,A}^{\vec{k}_P \vec{k}_A} = E_{ij,B}^{\vec{k}_P \vec{k}_A}$. With the same assumptions, the decay width becomes

$$\begin{aligned} \Gamma_h &= 2\pi \sum_{(i,j) \in \mathcal{F}} \sum_{\gamma \in \{A,B\}} \int_{\mathbb{R}^3} |\langle \gamma^1 \Phi_{ij}^{\vec{k}_P \vec{k}_A} | \hat{H}_1 | \gamma^1 \Phi_h^{\vec{k}_P} \rangle|^2 \\ &\quad \times \delta(E_h^{\vec{k}_P} - E_{ij,\gamma}^{\vec{k}_P \vec{k}_A}) d^3 k_A \\ &\approx 2\pi \sum_{(i,j) \in \mathcal{F}} \int_{\mathbb{R}^3} 2|v_h \bar{k}_A ij|^2 \delta(E_h^{\vec{k}_P} - E_{ij}^{\vec{k}_P \vec{k}_A}) d^3 k_A. \end{aligned} \quad (48)$$

As we assume the two-step model of Auger decay [6, 42], Γ_h is independent of the photoelectron momentum \vec{k}_P . In Eqs. (47) and (48), we mark explicitly the dependence on the hole orbital $h \in \mathcal{H}$. As all $h \in \mathcal{H}$ are from a single magnetic subshell, the $\Delta_{R,h}$ and the Γ_h agree for all $h \in \mathcal{H}$. Therefore, we may drop the dependence on h in what follows.

In the derivation of Eqs. (46), (47), and (48), we implicitly assume that $\bar{c}_P^{\vec{k}_P}(t)$ varies only slightly on time intervals $[t - \tau; t]$ for $t \in [-\infty; \infty]$ and a small $\tau > 0$ with respect to all time scales in the problem [27, 58]. Otherwise Eq. (46) would not be meaningful. We can integrate Eq. (45) formally,

$$\begin{aligned} \bar{c}_{ij}^{\vec{k}_P \vec{k}_A}(t) &= \int_{t-\tau}^t \bar{c}_{ij}^{\vec{k}_P \vec{k}_A}(t') dt' + \int_{-\infty}^{t-\tau} \bar{c}_{ij}^{\vec{k}_P \vec{k}_A}(t') dt' \\ &= \frac{1}{\sqrt{2}} \bar{v}(\vec{k}_A) \bar{c}_h^{\vec{k}_P}(t) \frac{e^{i(\frac{\bar{k}_A^2}{2} - \Omega_A - i\eta)t}}{\frac{\bar{k}_A^2}{2} - \Omega_A - i\eta}. \end{aligned} \quad (49)$$

Here, $e^{\eta t}$ with $\eta > 0$ ensures the initial condition $\bar{c}_A^{\vec{k}_P \vec{k}_A}(-\infty) = 0$ and the convergence of the integral where $\eta \rightarrow 0^+$ is performed after the integration. The last equality follows from $\int_{t-\tau}^t \bar{c}_A^{\vec{k}_P \vec{k}_A}(t') dt' = \bar{c}_A^{\vec{k}_P \vec{k}_A}(t) - \bar{c}_A^{\vec{k}_P \vec{k}_A}(t - \tau)$, where the term for $t - \tau$ cancels the second integral.

Our result for the Auger amplitude (49) is inserted into the expression for $w(\vec{k}_P, t)$ [the second term on the right-hand side of Eq. (44)] yielding

$$w(\vec{k}_P, t) = 2i \int_{\mathbb{R}^3} \frac{|\bar{v}(\vec{k}_A)|^2 e^{\eta t}}{\frac{\bar{k}_A^2}{2} - \Omega_A - i\eta} \bar{c}_h^{\vec{k}_P}(t) d^3 k_A. \quad (50)$$

With the decomposition [56]

$$\frac{1}{x - i\eta} = \text{Pr} \frac{1}{x} + i\pi\delta(x), \quad (51)$$

we obtain Eqs. (46), (47), and (48) after dropping the subscript h , eliminating the sum over final states and replacing the energies and two-electron matrix elements in Eqs. (47) and (48). In detail, we find

$$\Delta_R = \text{Pr} \int_{\mathbb{R}^3} \frac{2|\bar{v}(\vec{k}_A)|^2}{\Omega_A - \frac{\bar{k}_A^2}{2}} d^3 k_A, \quad (52)$$

and

$$\Gamma = 2\pi \int_{\mathbb{R}^3} 2|\bar{v}(\vec{k}_A)|^2 \delta\left(\Omega_A - \frac{\bar{k}_A^2}{2}\right) d^3 k_A. \quad (53)$$

A suitable value for the strength of the Auger decay matrix element (43) can be obtained from Eq. (53) via

$$Q_v = \sqrt{\frac{\Gamma_{\text{par}}}{\Gamma|_{Q_v=1}}}, \quad (54)$$

provided the decay width Γ_{par} is taken to be an (experimental) parameter.

C. Hole-state amplitude with laser dressing

In Secs. IV A and IV B, we disregarded laser dressing and focused on the EOMs with XUV light only. In the framework of Sec. III, we can easily incorporate laser dressing in the strong-field approximation [44] into our equations; the only change in our EOMs (44) and (45) concerns the time-dependent phase factors $i\frac{\bar{k}_A^2}{2}t$ which need to be replaced by Volkov phases $i\Phi_V(\vec{k}_P, t)$ [Eq. (36)]. Using relation (46), we decouple the hole amplitude from the Auger decay amplitude and recast Eq. (44) into

$$\begin{aligned} \bar{c}_P^{\vec{k}_P}(t) &= \frac{-i}{\sqrt{2}} \bar{d}(\vec{k}_P) \varepsilon_X(t) e^{i\Phi_V(\vec{k}_P, t)} e^{-i\Omega_P t} \\ &\quad + \left(-i\Delta_R - \frac{\Gamma}{2}\right) \bar{c}_P^{\vec{k}_P}(t), \end{aligned} \quad (55)$$

assuming that the Auger decay is uninfluenced by the laser and thus the second-order energy shift Δ_R [Eq. (52)] and the Auger decay rate Γ [Eq. (53)] are meaningful. The first-order ordinary differential equation (55) is solved analytically [56] yielding

$$\begin{aligned} \bar{c}_P^{\vec{k}_P}(t) &= \frac{-i}{\sqrt{2}} \bar{d}(\vec{k}_P) e^{-i(\Delta_R - i\frac{\Gamma}{2})t} \int_{-\infty}^t \varepsilon_X(t') \\ &\times e^{i\Phi_V(\vec{k}_P, t)} e^{i(\Delta_R - i\frac{\Gamma}{2} - \Omega_P)t'} dt'. \end{aligned} \quad (56)$$

To solve the time integration in Eq. (56), we expand the Volkov phase as in Eq. (41) and insert the inverse Fourier transform of the envelope of the XUV pulse (11),

$$\varepsilon_X(t') = \frac{1}{2\pi} \int_{-\infty}^{\infty} \tilde{\varepsilon}_X(\omega) e^{-i\omega t'} d\omega. \quad (57)$$

We obtain for the laser-dressed hole amplitude (56) the expression

$$\begin{aligned} \bar{c}_P^{\vec{k}_P}(t) &= \frac{-1}{2\sqrt{2}\pi} \bar{d}(\vec{k}_P) \sum_{m=-\infty}^{\infty} e^{im(\omega_L \Delta t - \frac{\pi}{2})} \\ &\times J_m\left(\vec{\alpha}_L \cdot \vec{k}_P, \frac{U_P}{2\omega_L}\right) \\ &\times \int_{-\infty}^{\infty} \frac{\tilde{\varepsilon}_X(\omega) e^{i(\frac{k_P^2}{2} + m\omega_L + U_P - \Omega_P - \omega)t}}{\frac{k_P^2}{2} + m\omega_L + U_P - \Omega_P + \Delta_R - \omega - i\frac{\Gamma}{2}} d\omega. \end{aligned} \quad (58)$$

For moderate laser intensities, we have $\frac{U_P}{2\omega_L} \approx 0$. Then, the generalized Bessel functions go over into ordinary Bessel functions [44, 55]. Further, the limit $\lim_{u, v \rightarrow 0} J_m(u, v) = \delta_{m,0}$ exists which completely removes the dependence of the equation on the laser for vanishing intensity. With this approximation, our expression (58) goes over into Smirnova *et al.*'s [26, 59] Eq. (15).

D. Laser-dressed Auger electron spectrum

The amplitude to observe an Auger electron with momentum \vec{k}_A for a photoelectron with momentum \vec{k}_P at time t is found by integrating Eq. (45) from $-\infty$ to t . Beforehand, expression (45) needs to be adapted for laser dressing by replacing $i\frac{k_A^2}{2}t$ with $i\Phi_V(\vec{k}_A, t)$ after which we insert the hole-state amplitude (58). We obtain the

following closed-form expression:

$$\begin{aligned} \bar{c}_A^{\vec{k}_P \vec{k}_A}(t) &= \frac{-i}{4\pi} \bar{d}(\vec{k}_P) \bar{v}(\vec{k}_A) \sum_{m=-\infty}^{\infty} e^{im(\omega_L \Delta t - \frac{\pi}{2})} \\ &\times J_m\left(\vec{\alpha}_L \cdot \vec{k}_P, \frac{U_P}{2\omega_L}\right) \\ &\times \int_{-\infty}^{\infty} \frac{\tilde{\varepsilon}_X(\omega)}{\frac{k_P^2}{2} + m\omega_L + U_P - \Omega_P + \Delta_R - \omega - i\frac{\Gamma}{2}} \\ &\times \int_{-\infty}^t e^{i(\frac{k_P^2}{2} + m\omega_L + U_P - \Omega_P - \Omega_A - \omega)t'} \\ &\times e^{i\Phi_V(\vec{k}_A, t')} dt' d\omega. \end{aligned} \quad (59)$$

We are only interested in the Auger electron spectrum after the XUV pulse is over and the induced hole amplitude has decayed. Therefore, after expanding the Volkov phase (41), we let $t \rightarrow \infty$ and simplify the time integration in Eq. (59) by observing that

$$\delta(\omega - \omega') = \frac{1}{2\pi} \int_{-\infty}^{\infty} e^{i(\omega - \omega')t'} dt' \quad (60)$$

is a representation for Dirac's δ distribution [32, 56]. Finally, we obtain the laser-dressed Auger amplitude,

$$\begin{aligned} \bar{c}_A^{\vec{k}_P \vec{k}_A}(\infty) &= \frac{i}{2} \bar{d}(\vec{k}_P) \bar{v}(\vec{k}_A) \sum_{m, n=-\infty}^{\infty} e^{i(m+n)(\omega_L \Delta t - \frac{\pi}{2})} \\ &\times J_m\left(\vec{\alpha}_L \cdot \vec{k}_P, \frac{U_P}{2\omega_L}\right) J_n\left(\vec{\alpha}_L \cdot \vec{k}_A, \frac{U_P}{2\omega_L}\right) \\ &\times S\left(\frac{k_P^2}{2} + m\omega_L + U_P, \frac{k_A^2}{2} + n\omega_L + U_P\right), \end{aligned} \quad (61)$$

with the line shape function

$$S(\omega_P, \omega_A) = \frac{\tilde{\varepsilon}_X(\omega_P + \omega_A - \Omega_P - \Omega_A)}{\omega_A - \Omega_A - \Delta_R + i\frac{\Gamma}{2}}, \quad (62)$$

which depends only on the absolute values of the momenta \vec{k}_P and \vec{k}_A . Formula (61) goes over into Eq. (18) in Ref. [26]—apart from a factor $\frac{1}{2}$ in our expression—by setting $U_P = 0$, replacing the generalized Bessel functions by ordinary ones and removing the dependence on the laser for the photoelectrons by using $J_m(0) = \delta_{m,0}$.

We are now in a position to determine the laser-dressed Auger electron spectrum where we consider the case that the photoelectron is not observed. Therefore, we integrate the probability density $|\bar{c}_A^{\vec{k}_P \vec{k}_A}(\infty)|^2$ [Eqs. (61) and (62)] over all possible photoelectron momenta to eliminate this degree of freedom. This yields for the probability density [32] to observe an Auger electron with momentum vector \vec{k}_A ,

$$P_A(\vec{k}_A) = \int_{\mathbb{R}^3} |\bar{c}_A^{\vec{k}_P \vec{k}_A}(\infty)|^2 d^3k_P. \quad (63)$$

E. xuv absorption cross section of laser-dressed atoms

The probability of finding an atom in the ground state is given in terms of the ground-state amplitude $\bar{c}_0(t)$ in the wave packet (23) by

$$\mathcal{P}_0(t) = |\bar{c}_0(t)|^2 = \bar{c}_0^*(t) \bar{c}_0(t). \quad (64)$$

Consequently, the negative of the XUV-absorption rate [38] is

$$\begin{aligned} -\Gamma_X(t) &= \dot{\mathcal{P}}_0(t) = \dot{\bar{c}}_0^*(t) \bar{c}_0(t) + \bar{c}_0^*(t) \dot{\bar{c}}_0(t) \\ &\approx \dot{\bar{c}}_0^*(t) + \dot{\bar{c}}_0(t) \\ &= 2 \operatorname{Re} \dot{\bar{c}}_0(t) = 2 \operatorname{Im} [i \dot{\bar{c}}_0(t)]. \end{aligned} \quad (65)$$

The center line follows from the weakness of XUV absorption, i.e., $\bar{c}_0(t) \approx 1$ for all t . The rate of change of the ground-state amplitude follows from the first EOM (24); adapted for the essential-states model with laser dressing, it reads

$$\dot{\bar{c}}_0(t) = \frac{-i}{\sqrt{2}} \int_{\mathbb{R}^3} \bar{d}^*(\vec{k}_P) \varepsilon_X(t) e^{i\Omega_P t} e^{-i\Phi_V(\vec{k}_P, t)} \bar{c}_P^{\vec{k}_P}(t) d^3 k_P. \quad (66)$$

Inserting this EOM into Eq. (65), expanding the Volkov phase factor using Eq. (41), and inserting the laser-dressed hole-state amplitude (58), we obtain the rate

$$\begin{aligned} \Gamma_X(t) &= -2 \operatorname{Im} [i \dot{\bar{c}}_0(t)] = \frac{1}{2\pi} \varepsilon_X(t) \sum_{m, n=-\infty}^{\infty} \int_{\mathbb{R}^3} J_m(\vec{\alpha}_L \cdot \vec{k}_P, \frac{U_P}{2\omega_L}) J_n(\vec{\alpha}_L \cdot \vec{k}_P, \frac{U_P}{2\omega_L}) \\ &\quad \times |\bar{d}(\vec{k}_P)|^2 \int_{-\infty}^{\infty} \operatorname{Im} \left[\frac{\tilde{\varepsilon}_X(\omega) e^{-i\omega t} e^{i(n-m)[\omega_L(t+\Delta t) - \frac{\pi}{2}]} }{\frac{\vec{k}_P^2}{2} + n\omega_L + U_P - \Omega_P + \Delta_R - \omega - i\frac{\Gamma}{2}} \right] d\omega d^3 k_P. \end{aligned} \quad (67)$$

The absorption rate (67) in conjunction with the flux $J_X = \frac{I_{X,0}}{\omega_X}$ at the XUV (peak) intensity $I_{X,0}$ with photon energy ω_X allows one to obtain the XUV photoabsorption cross section [60] via

$$\sigma = \frac{\Gamma_X}{J_X}. \quad (68)$$

Note that for a continuous-wave approximation of monochromatic radiation, we have for the XUV field strength $\tilde{\varepsilon}_X(\omega) = \tilde{\varepsilon}_{X,0} \delta(\omega)$ and $\varepsilon_X(t) = E_{X,0} = \sqrt{8\pi\alpha I_{X,0}} = \text{const}$ for all t . The relation between time- and frequency-domain field amplitudes follows from Eq. (57) and is $E_{X,0} = \frac{1}{2\pi} \tilde{\varepsilon}_{X,0}$. For large t , terms with $m \neq n$ oscillate rapidly in the absorption rate (67). We discard these terms and retain only the constant terms with $m = n$. This leads to the expression

$$\sigma(\omega_X) = 8\pi\alpha\omega_X \sum_{m=-\infty}^{\infty} \int_{\mathbb{R}^3} J_m(\vec{\alpha}_L \cdot \vec{k}_P, \frac{U_P}{2\omega_L})^2 \operatorname{Im} \left[\frac{|\bar{d}(\vec{k}_P)|^2}{E^+ + \frac{\vec{k}_P^2}{2} + m\omega_L + U_P - E_0 + \Delta_R - \omega_X - i\frac{\Gamma}{2}} \right] d^3 k_P, \quad (69)$$

by expanding $\Omega_P = E_0 - E^+ + \omega_X$. For vanishing laser intensity, the structure of this equations becomes the same as from Eq. (40) in Ref. [38]. There, however, Δ_R was not accounted for.

Similarly to Eq. (54), a suitable value for the strength of the dipole matrix element (42) can be obtained from Eq. (69), omitting laser dressing, via

$$Q_d = \sqrt{\frac{\sigma_{\text{par}}(\omega_{\text{par}})}{\sigma(\omega_{\text{par}})|_{Q_d=1}}}, \quad (70)$$

provided the cross section $\sigma_{\text{par}}(\omega_{\text{par}})$ at an energy ω_{par} in the range of energies of interest or close to the range is taken as a (experimental) parameter.

F. Laser-dressed photoelectron spectrum

We determined the rate with which XUV light is absorbed $\Gamma_X(t)$ [Eq. (65)] in Sec. IV E. The rate was derived under the premise of weak XUV absorption which allowed us to approximate the ground-state amplitude by $\bar{c}_0(t) \approx 1$ for all t . Therefore, $|\bar{c}_0(t)|^2$ cannot be used to obtain the probability with which photoelectrons are ejected. Instead, we need to integrate the rate

$$\mathcal{P}_P(t) = \int_{-\infty}^t \Gamma_X(t') dt' = -2 \int_{-\infty}^t \operatorname{Im} [i \dot{\bar{c}}_0(t')] dt'. \quad (71)$$

In expression (71), we insert the ground-state amplitude rate of change (66) and the laser-dressed hole-state amplitude (58) and expand the Volkov phase factor (41) to

obtain the probability

$$\mathcal{P}_P(t) = \frac{1}{2\pi} \sum_{m,n=-\infty}^{\infty} \int_{\mathbb{R}^3} J_m(\vec{\alpha}_L \cdot \vec{k}_P, \frac{U_P}{2\omega_L}) J_n(\vec{\alpha}_L \cdot \vec{k}_P, \frac{U_P}{2\omega_L}) \int_{-\infty}^t \varepsilon_X(t') \int_{-\infty}^{\infty} \text{Im} \left[\tilde{\varepsilon}_X(\omega) \right. \\ \left. \times \frac{|\tilde{d}(\vec{k}_P)|^2 e^{-i\omega t} e^{i(n-m)[\omega_L(t+\Delta t) - \frac{\pi}{2}]} }{\frac{k_P^2}{2} + n\omega_L + U_P - \Omega_P + \Delta_R - \omega - i\frac{\Gamma}{2}} \right] d\omega dt' d^3k_P. \quad (72)$$

Letting $t \rightarrow \infty$, replacing the real-valued $\varepsilon_X(t')$ by the complex conjugate of Eq. (57), and omitting the integration over \vec{k}_P , we find the probability density for photoelectron ejection by the XUV pulse. The time integration yields a δ distribution (60) of the form $\delta(\omega' - \omega + (n - m)\omega_L)$. Replacing $\tilde{m} \equiv n - m$, we arrive at the probability density

$$\tilde{\mathcal{P}}_P(\vec{k}_P) \equiv \frac{1}{2\pi} |\tilde{d}(\vec{k}_P)|^2 \sum_{\tilde{m}=-\infty}^{\infty} \sum_{n=-\infty}^{\infty} J_{n-\tilde{m}}(\vec{\alpha}_L \cdot \vec{k}_P, \frac{U_P}{2\omega_L}) J_n(\vec{\alpha}_L \cdot \vec{k}_P, \frac{U_P}{2\omega_L}) \\ \times \text{Im} \left[\int_{-\infty}^{\infty} \frac{e^{i\tilde{m}[\omega_L \Delta t - \frac{\pi}{2}]} \tilde{\varepsilon}_X^*(\omega - \tilde{m}\omega_L) \tilde{\varepsilon}_X(\omega)}{\frac{k_P^2}{2} + n\omega_L + U_P - \Omega_P + \Delta_R - \omega - i\frac{\Gamma}{2}} d\omega \right]. \quad (73)$$

The photoelectron spectrum depends on the Fourier transform of the XUV field envelope at ω and at $\omega - \tilde{m}\omega_L$. This functional dependence indicates interference effects between channels with a different number of laser photons provided that the XUV field envelope has sufficient width.

V. ELECTRONIC STRUCTURE

The theory of Secs. II, III, and IV treated the electronic structure of an atom as an abstract quantity which was represented by the orbital energies in \hat{H}_{HFS} [Eq. (4)], the one-electron matrix elements in \hat{H}_{CH} [Eq. (5)], the dipole matrix elements in \hat{H}_X [Eq. (9)], and the two-electron matrix elements in \hat{H}_{ee} [Eq. (7)]. Programs exist to carry out the Hartree-Fock-Slater approximation [48, 49] and compute the required one- and two-electron matrix elements. To evaluate the essential-states model of Sec. IV, however, we use a much simpler model approach in terms of scaled hydrogenic functions for the atomic orbitals. This treatment follows Refs. [25, 26, 27]. The parametrization of the model corrects to a large extent for inaccuracies in the orbital energies and the matrix elements. If the results of the essential-states model depended sensitively on the electronic structure, then due to the substantial simplifications made, its physical predictions would be untrustworthy. Despite the use of approximate orbitals, the equations derived in this section are completely general and an *ab initio* evaluation in terms of Hartree-Fock-Slater orbitals is feasible.

We use hydrogenic wave functions to model the spatial atomic orbitals in spherical polar coordinates $\tilde{\varphi}_i(r, \vartheta, \varphi) = R_{n_i l_i}(r) Y_{l_i m_i}(\vartheta, \varphi)$ [32]. Here, n_i ,

l_i , and m_i are the principal, orbital angular momentum, and magnetic quantum number, respectively, of orbital $i \in \{1, \dots, Z/2\}$. The radial part is $R_{n_i l_i}(r)$ and the angular dependence is described by spherical harmonics $Y_{l_i m_i}(\vartheta, \varphi)$. We scale the hydrogenic wave functions such that their energy $E_{n_i} = -\frac{Z^2}{2n_i^2}$ matches the energy ε_i of the corresponding orbital in the chosen atom [25, 27]. For this purpose we use an effective charge

$$Z_{\text{eff},i} = n_i \sqrt{-2\varepsilon_i}. \quad (74)$$

This scaling also adjusts the spatial extend of the orbital appropriately.

A. Dipole matrix elements

The dipole matrix elements for XUV absorption (12) are given by the promoted wave function in momentum space [32, 61],

$$d_{\vec{k}_P h} = \frac{1}{(2\pi)^{3/2}} \int_{\mathbb{R}^3} e^{-i\vec{k} \cdot \vec{r}} z \varphi_h(\vec{r}) d^3r, \quad (75)$$

with $\vec{r} \cdot \vec{e}_X = z$. We use an atomic orbital $\varphi_h(\vec{r})$ for the vacancy created by photoionization and the spatial part $\varphi_{P,\vec{k}}(\vec{r}, 0)$ of a plane wave (30). This comprises also the case when laser dressing is considered because the laser dressing manifests itself exclusively [54] in the time-dependent Volkov phase (35). We use the Rayleigh expansion [62] of the plane waves in Eq. (75),

$$e^{i\vec{k} \cdot \vec{r}} = 4\pi \sum_{l=0}^{\infty} \sum_{m=-l}^l i^l Y_{lm}^*(\vartheta_k, \varphi_k) j_l(kr) Y_{lm}(\vartheta, \varphi). \quad (76)$$

The directions of \vec{k} and \vec{r} are specified by the polar angles ϑ_k , φ_k and ϑ , φ , respectively. Here, j_l denotes a

spherical Bessel function [56]. We arrive at the dipole matrix element (75) in spherical polar coordinates,

$$\tilde{d}_h(k_P, \vartheta_{k_P}, \varphi_{k_P}) = 2\sqrt{\frac{2}{3}} \sum_{\substack{l \in \{l_h^{-1}, l_h+1\} \\ l \geq 0}} (-i)^l \mathcal{Y}(l_h, 1, l; m_h, 0, m_h) Y_{l m_h}(\vartheta_{k_P}, \varphi_{k_P}) \mathcal{D}_{n_h l_h}^{(l)}(k_P). \quad (77)$$

Corresponding to orbital h , we have the principal n_h , orbital angular momentum l_h , and magnetic m_h quantum numbers. The angular integral is

$$\begin{aligned} \mathcal{Y}(l_1, l_2, l_3; m_1, m_2, m_3) &= \int_{4\pi} Y_{l_3 m_3}^*(\Omega) Y_{l_2 m_2}(\Omega) Y_{l_1 m_1}(\Omega) d\Omega \\ &= \sqrt{\frac{(2l_1+1)(2l_2+1)}{4\pi(2l_3+1)}} C(l_1, l_2, l_3; m_1, m_2, m_3) C(l_1, l_2, l_3; 0, 0, 0), \end{aligned} \quad (78)$$

where $C(l_1, l_2, l_3; m_1, m_2, m_3)$ is a Clebsch-Gordan coefficient [62]. The integral restricts the accessible angular momenta and magnetic quantum numbers in the photoionization process. The radial dipole matrix elements are

$$\mathcal{D}_{n_h l_h}^{(l)}(k_P) = \int_0^\infty j_l(k_P r) r^3 R_{n_h l_h}(r) dr, \quad (79)$$

in terms of the radial part $R_{n_h l_h}(r)$ of the atomic orbital h .

B. Auger transition matrix elements

Auger decay is mediated by the two-electron matrix element,

$$v_{h \vec{k}_A ij} \equiv \tilde{\chi}_h^{ij}(\vec{k}_A) = \frac{1}{(2\pi)^{3/2}} \int_{\mathbb{R}^3} e^{-i\vec{k}_A \cdot \vec{r}} \chi_h^{ij}(\vec{r}) d^3r. \quad (80)$$

Here, $\chi_h^{ij}(\vec{r})$ and $\tilde{\chi}_h^{ij}(\vec{k}_A)$ are the configuration space and momentum space Auger electron wave functions, respectively [25, 32]. With the two-electron repulsion \hat{h}_{ee} [Eq. (8)], the configuration space Auger electron wave functions reads

$$\chi_h^{ij}(\vec{r}) = \varphi_j(\vec{r}) \int_0^\infty \int_{4\pi} \tilde{\varphi}_h^*(r', \Omega') \hat{h}_{ee} \tilde{\varphi}_i(r', \Omega') r'^2 dr' d\Omega'. \quad (81)$$

To simplify \hat{h}_{ee} , we replace it by the Laplace expansion [63],

$$\frac{1}{|\vec{r} - \vec{r}'|} = \sum_{l=0}^\infty \frac{4\pi}{2l+1} \varrho_l(r, r') \sum_{m=-l}^l Y_{lm}^*(\vartheta', \varphi') Y_{lm}(\vartheta, \varphi), \quad (82)$$

with the decomposition

$$\varrho_l(r, r') = \frac{r'^l}{r^{l+1}} \theta(r - r') + \frac{r^l}{r'^{l+1}} \theta(r' - r), \quad (83)$$

for the radial dependence, where θ is the Heaviside step function with $\theta(0) = \frac{1}{2}$. The wave function of the Auger electron is in spherical polar coordinates,

$$\begin{aligned} \tilde{\chi}_h^{ij}(r, \vartheta, \varphi) &= \tilde{\varphi}_j(r, \vartheta, \varphi) \sum_{\substack{l \text{ with } \Delta(l_h, l, l_i) \\ l_i + l_h + l \text{ even}}} \frac{4\pi}{2l+1} \\ &\times \mathcal{Y}(l_h, l, l_i; m_h, m_i - m_h, m_i) \\ &\times \mathcal{R}_{n_h l_h, n_i l_i, l}^{(1)}(r) Y_{l m_i - m_h}(\vartheta, \varphi). \end{aligned} \quad (84)$$

The symbol $\Delta(l_h, l, l_i)$ represents the triangular condition for which Clebsch-Gordan coefficients do not vanish [62]. The radial dependence in Eq. (84) is expressed by

$$\mathcal{R}_{n_h l_h, n_i l_i, l}^{(1)}(r) = \int_0^\infty R_{n_h l_h}(r') \varrho_l(r, r') R_{n_i l_i}(r') r'^2 dr'. \quad (85)$$

We would like to calculate the momentum space representation (80) of the Auger electron wave function (84) [32, 61]. The plane wave is expanded in terms of spherical Bessel functions (76),

$$\begin{aligned} \tilde{\chi}_h^{ij}(k_A, \vartheta_{k_A}, \varphi_{k_A}) &= 4\sqrt{2\pi} \sum_{\substack{l \text{ with } \Delta(l_h, l, l_i) \\ l_i + l_h + l \text{ even}}} \frac{1}{2l+1} \\ &\times \mathcal{Y}(l_h, l, l_i; m_h, m_i - m_h, m_i) \sum_{\substack{l' \text{ with } \Delta(l, l', l_j) \\ l + l' + l_j \text{ even}}} (-i)^{l'} \\ &\times \mathcal{Y}(l, l_j, l'; m_i - m_h, m_j, m_i + m_j - m_h) \\ &\times \mathcal{R}_{n_h l_h, n_i l_i, n_j l_j, l, l'}^{(2)}(k_A) Y_{l' m_i + m_j - m_h}(\vartheta_{k_A}, \varphi_{k_A}) \end{aligned} \quad (86)$$

with

$$\mathcal{R}_{n_h l_h, n_i l_i, n_j l_j, l, l'}^{(2)}(k_A) = \int_0^\infty j_{l'}(k_A r) \mathcal{R}_{n_h l_h, n_i l_i, l}^{(1)}(r) \times R_{n_j l_j}(r) r^2 dr. \quad (87)$$

We can decompose $\mathcal{R}_{n_h l_h, n_i l_i, n_j l_j, l, l'}^{(2)}(k_A)$ (87) into a product of two independent one-dimensional integrals by

assuming the product ansatz

$$\varrho_l(r, r') = \varrho_{1,l}(r) \varrho_{2,l}(r') \quad (88)$$

for the radial dependence (83). This simplifies our task to evaluate Eq. (87) greatly. It becomes

$$\mathcal{R}_{n_h l_h, n_i l_i, n_j l_j, l, l'}^{(2)}(k_A) = \mathcal{R}_{n_j l_j, l, l'}^{(3)}(k_A) \mathcal{R}_{n_h l_h, n_i l_i, l}^{(4)}, \quad (89)$$

with

$$\mathcal{R}_{n_j l_j, l, l'}^{(3)}(k_A) = \int_0^\infty j_{l'}(k_A r) \varrho_{1,l}(r) R_{n_j l_j}(r) r^2 dr \quad (90)$$

and

$$\mathcal{R}_{n_h l_h, n_i l_i, l}^{(4)} = \int_0^\infty R_{n_h l_h}(r') \varrho_{2,l}(r') R_{n_i l_i}(r') r'^2 dr'. \quad (91)$$

VI. COMPUTATIONAL DETAILS

All computations were carried out with MATHEMATICA [64]. In our essential-states model of Auger decay, the set of hole orbitals \mathcal{H} comprises all five $3d$ orbitals of krypton. The set of final states \mathcal{F} consists of pairs of orbitals, the first is the $4s$ orbital and the second is a $4p$ orbital with magnetic quantum number $m \in \{-1, 0, 1\}$. The atomic orbital energies of krypton are taken from Ref. [27]: $\varepsilon_{3d} = -70$ eV, $\varepsilon_{4s} = -15$ eV, and $\varepsilon_{4p} = -15$ eV. The effective charges (74) assume the values $Z_{3d} = 6.8$, $Z_{4s} = 4.2$, and $Z_{4p} = 4.2$. The orbital energies lead us to state energies (disregarding $\hat{H}_{CH} + \hat{H}_{ee}$) via Eqs. (16), (17), and (18). This yields, for XUV photons with $\omega_X = 90$ eV, a nominal photoelectron energy of $\Omega_P = E_0 - E^+ + \omega_X = \varepsilon_{3d} + \omega_X = 20$ eV [26, 27]. We obtain a nominal Auger electron energy of $\Omega_A = E^+ - E^{++} = \varepsilon_{4s} + \varepsilon_{4p} - \varepsilon_{3d} = 40$ eV. The Auger decay width of a $3d$ hole in krypton is *artificially* set to $\Gamma_{\text{broad}} = 1.3$ eV, which corresponds to a decay time of 500 as in accord with the data in Fig. 3 in Ref. [26]. We use this much shorter decay time to show the coherence in the laser-dressed Auger spectrum. The experimental value for the decay width is $\Gamma_{\text{expt}} = 88$ meV which corresponds to a decay time of 7.5 fs [18].

With an approximation which we discuss below [see Eq. (94)] for the radial dependence (88), we determine the strengths of the dipole (42) and Auger decay (43) matrix elements. Using the decay width $\Gamma|_{Q_d=1}$ from Eq. (53), we find from Eq. (54) the strengths $Q_{v,\text{expt}} = 1.10$ with Γ_{expt} and $Q_{v,\text{broad}} = 4.25$ with Γ_{broad} . The corresponding energy shifts follow from Eq. (52). They are $\Delta_{R,\text{expt}} = -0.90$ eV for $Q_{v,\text{expt}}$ and $\Delta_{R,\text{broad}} = -13.53$ eV for $Q_{v,\text{broad}}$. For a good agreement with the reference data [see Fig. 6 below], we employ the value $Q_v = 3.1$ and the shift $\Delta_R = -0.68$ eV. However, we set $\Delta_R = 0$ in all our computations because we have

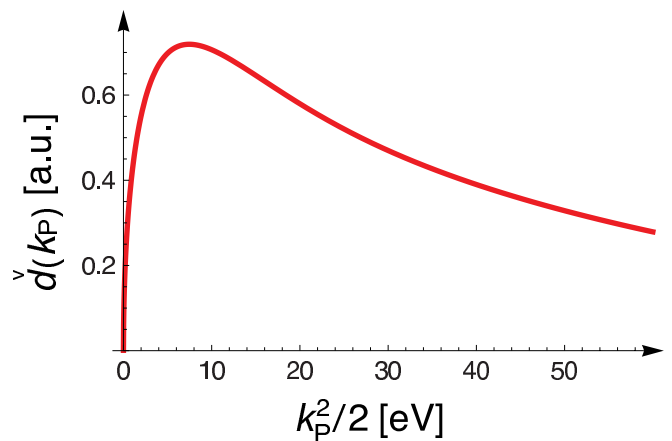


FIG. 3: (Color online) Spherically integrated rms dipole matrix element $\check{d}(k_P)$ [Eq. (93)] for the description of $3d$ photoionization of a krypton atom in the essential-states model of Sec. IV.

chosen the orbital energies such that they correctly reproduce the (experimental) Auger and photoelectron energies. The photoionization cross section of the krypton $3d$ subshell for 20 eV photoelectron energy in Hartree-Fock-Slater approximation [65] is read off of graph I in Ref. [66]; it is about $\sigma_{\text{HFS}} = 1.5$ Mbarn. The cross section without laser dressing $\sigma(\omega_X)|_{Q_d=1}$ is determined from Eq. (69) using Γ_{expt} and letting $\Delta_R = 0$. With Eq. (70), we obtain a dipole strength of $Q_d = 0.26$.

We use a XUV light pulse which has a Gaussian envelope with peak intensity $I_{X,0}$ at $t = 0$ and a full width at half maximum duration of $\tau_X = 500$ as

$$I_X(t) = I_{X,0} e^{-4 \ln 2 \left(\frac{t}{\tau_X}\right)^2}. \quad (92)$$

The XUV electric-field envelope in Eq. (11) follows from $\epsilon_X(t) = \sqrt{8\pi \alpha I_X(t)}$; its Fourier transform is also a Gaussian [56].

VII. RESULTS AND DISCUSSION

We devote this section to a computational study of our essential-states model and its parameters applied to $M_{4,5}N_1N_{2,3}$ Auger decay in krypton [16, 17, 18, 19]. It is motivated by a previous experiment [14] which focused on the line group around 40 eV and related theoretical studies [25, 26, 27]. We assess the accuracy of the approximations made in our essential-states model and compare with existing literature results. In future work [40], we will explore laser-dressed Auger decay extensively. Additionally, we present the laser-dressed Auger spectrum for a much higher dressing-laser intensity than what has been used so far.

To begin with, let us discuss the results for the rms matrix elements (42) and (43) of the essential-states model. First, XUV absorption is determined by the rms dipole

matrix element in spherical polar coordinates (42) which is determined from the $\tilde{d}_h(k_P, \vartheta_{k_P}, \varphi_{k_P})$ [Eq. (77)] for all $h \in \mathcal{H}$. We take its modulus squared and integrate over the full solid angle to obtain the spherically integrated rms dipole matrix element,

$$\check{d}(k_P) = \sqrt{\int_{4\pi} |\tilde{d}(k_P, \Omega_{k_P})|^2 d\Omega_{k_P}}. \quad (93)$$

It is plotted in Fig. 3. After a steep rise at the edge (zero photoelectron momentum), it decays smoothly. Around the nominal photoelectron energy of $\Omega_P = 20$ eV, the dependence of $\check{d}(k_P)$ on k_P is weak. Additionally, quantities such as the line shape function (62) decrease rapidly as soon as $\frac{k_P^2}{2}$ deviates appreciably from Ω_P .

Second, Auger decay is mediated by the rms two-electron matrix element (43). To construct it, we need the direct two-electron matrix element $\check{\chi}_h^{ij}(k_A, \vartheta_{k_A}, \varphi_{k_A})$ [Eq. (86)] for all $h \in \mathcal{H}$. The rms matrix element in spherical polar coordinates is then denoted by $\tilde{v}(k_A, \vartheta_{k_A}, \varphi_{k_A})$. We examine three cases for the radial dependence (83) and (88). This provides us with a good way to assess the quality of our approximation. First, following Refs. [25, 27], we use

$$\varrho_l(r, r') = \frac{r'^l}{r^{l+1}}. \quad (94)$$

Second, we examine the reverse case,

$$\varrho_l(r, r') = \frac{r^l}{r'^{l+1}}, \quad (95)$$

and, finally, the exact case (83). For comparison with Refs. [25, 26, 27] and for computational efficiency, we will use the crude approximation (94) throughout.

We display the rms two-electron matrix element $\tilde{v}(k_A, 0, 0)$ in Fig. 4 with the viewing direction along the z axis which, in turn, is the direction of the linear XUV and laser polarization vectors. Our choice of direction agrees with Ref. [26]. The dependence around the nominal Auger energy of $\Omega_A = 40$ eV—i.e., over the range plotted in Fig. 7—is weak.

To assess the impact of our omission of the two-electron exchange matrix element $v_{h\tilde{k}_A j i}$ in the essential-states model of Sec. IV, we compute its rms value in spherical polar coordinates $\tilde{v}_X(k_A, \vartheta_{k_A}, \varphi_{k_A})$. It is displayed in Fig. 5 along the z axis, $\tilde{v}_X(k_A, 0, 0)$, for the approximations in Eqs. (94) and (95). The values of $\tilde{v}_X(k_A, 0, 0)$ in our momentum range of interest are roughly one order of magnitude smaller than the corresponding values of the direct matrix element at the same momentum in Fig. 4 for the approximation Eq. (94). The other case [Eq. (95)] yields very large value for $\tilde{v}_X(k_A, 0, 0)$. Particularly, these values are much larger than corresponding values for $\tilde{v}(k_A, 0, 0)$ which is unphysical. This comparison underscores that Eq. (94) represents a reasonable approximation to the full Eq. (83) while Eq. (95) does not.

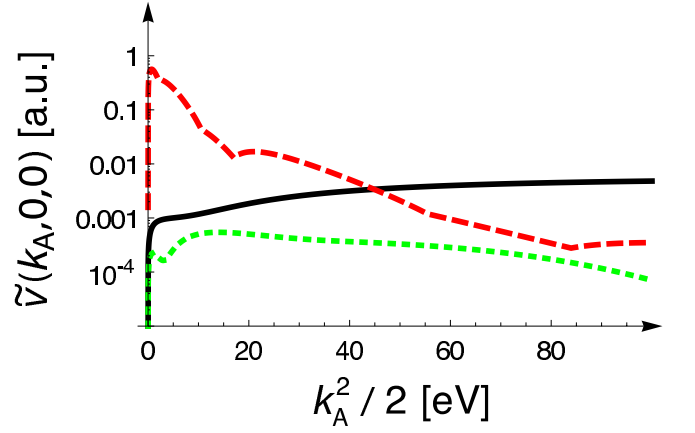


FIG. 4: (Color online) The rms two-electron direct matrix element for krypton 3d-hole Auger decay $\tilde{v}(k_A, 0, 0)$ of the essential-states model of Sec. IV. Using the first radial dependence (94) to find $\tilde{v}(k_A, 0, 0)$ yields the solid black line; the second radial dependence (95) gives the dashed red line; and the exact result (83) is represented by the dotted green line.

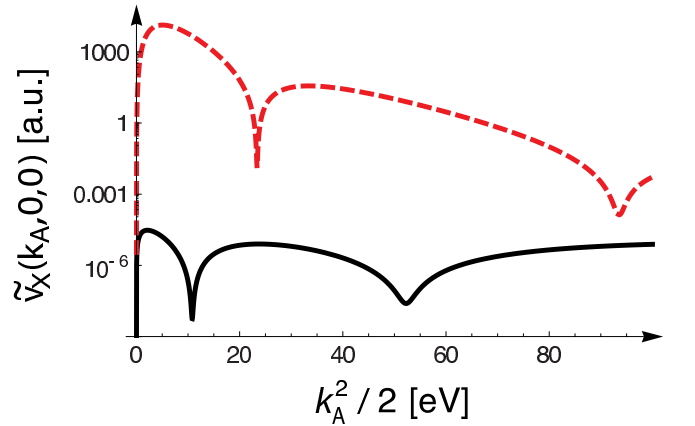


FIG. 5: (Color online) The rms two-electron exchange matrix element $\tilde{v}_X(k_A, 0, 0)$ for krypton 3d-hole Auger decay. See Fig. 4 for details.

$I_{L,0}$ [$\frac{\text{W}}{\text{cm}^2}$]	10^{10}	10^{11}	10^{12}	10^{13}	10^{14}
\mathcal{A}_L [a.u.]	0.0094	0.030	0.094	0.30	0.94
$E_{L,0}$ [a.u.]	0.00053	0.0017	0.0053	0.017	0.053
U_P [eV]	0.00060	0.0060	0.060	0.60	6.0
α_L [\AA]	0.087	0.28	0.87	2.8	8.7
$\frac{U_P}{2\omega_L}$	0.00019	0.0019	0.019	0.19	1.9

TABLE I: Parameters for an 800nm dressing laser. The vector potential amplitude \mathcal{A}_L (31), the electric-field amplitude $E_{L,0}$ (32), the ponderomotive potential U_P (37), the magnitude of the maximum excursion α_L (38), and the second argument in generalized Bessel functions for a broad range of intensities $I_{L,0}$.

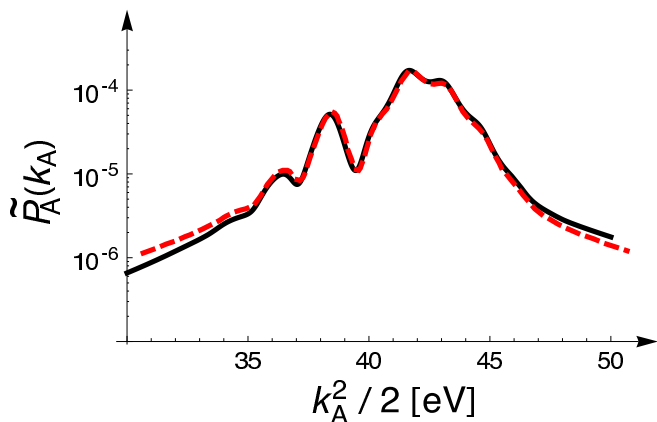


FIG. 6: (Color online) Auger electron spectrum (63) of laser-dressed krypton $3d$ -hole decay with an artificial width of $\Gamma_{\text{broad}} = 1.3 \text{ eV}$ for a dressing-laser intensity of $5 \times 10^{11} \frac{\text{W}}{\text{cm}^2}$. The solid black line was determined using our theory; the dashed red line is the solid curve of Fig. 3 in Ref. [26] scaled by a factor of $E_{X,0}^2 = 2.9 \times 10^{-4} \text{ a.u.}$ and shifted by -0.68 eV .

We need to specify and characterize the XUV and optical light fields next. A present-day attosecond-pulse light source typically has a XUV peak intensity of at most $I_{X,0} = 10^{11} \frac{\text{W}}{\text{cm}^2}$ at a photon energy of $\omega_X = 90 \text{ eV}$. The resulting ponderomotive potential (37) is $1.8 \mu\text{eV}$ with a magnitude of maximum excursion (38) of 8.2 fm . Clearly, the impact of the XUV field on photo- and Auger electrons can be omitted in excellent approximation. However, this approximation does not hold for the dressing laser—typically a Ti:sapphire laser system with near-infrared (NIR) light of a wavelength of 800 nm and a photon energy of $\omega_X = 1.55 \text{ eV}$ —which delivers a large range of laser intensities. Exemplary data are given in Table I. For lower intensities—up to $10^{12} \frac{\text{W}}{\text{cm}^2}$ —the ponderomotive potential (37) and the vector potential amplitude \mathcal{A}_L [Eq. (31)] are small in relation to the laser photon energy. Also \mathcal{A}_L is negligible compared with the momentum of the photo- and Auger electrons. Therefore, we may neglect the influence of the ponderomotive potential U_P . Specifically, this amounts to replacing generalized by ordinary Bessel functions in equations such as (36), (63), (69), and (73). For the Auger spectrum (63) this was done in Refs. [25, 27] and was done also in this paper for laser intensities up to $10^{12} \frac{\text{W}}{\text{cm}^2}$. This approximation is assessed by comparing Auger spectra from the expression using generalized Bessel functions (40) with spectra from the corresponding expression using ordinary Bessel functions. Excellent agreement is found.

Finally, we are in the position to put together all ingredients to compute the laser-dressed Auger electron spectrum (63) in spherical polar coordinates of krypton $3d$ hole decay [67] $\tilde{\mathcal{P}}_A(k_A, \vartheta_{k_A}, \varphi_{k_A})$ integrated over the azimuth angle $\tilde{\mathcal{P}}_A(k_A) = 2\pi \tilde{\mathcal{P}}_A(k_A, 0, 0)$. As a verification of our solution, we compute the Auger spectrum in Fig. 6 for a dressing-laser intensity of $5 \times 10^{11} \frac{\text{W}}{\text{cm}^2}$ as

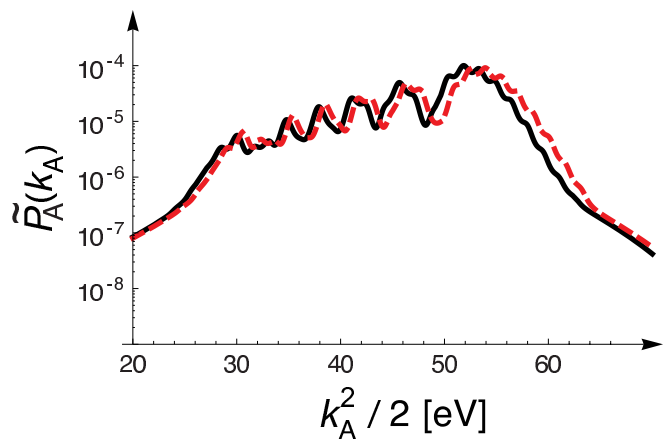


FIG. 7: (Color online) Auger electron spectrum (63) of laser-dressed krypton $3d$ -hole decay for an artificial width of $\Gamma_{\text{broad}} = 1.3 \text{ eV}$ and a dressing-laser intensity of $10^{13} \frac{\text{W}}{\text{cm}^2}$. The solid black line was determined using generalized Bessel functions (40); the dashed red line was obtained neglecting U_P and using ordinary Bessel functions.

in Fig. 3 in Ref. [26]. Our result agrees very well with the one in Ref. [26] apart from an overall scaling factor of $E_{X,0}^2 = 2.9 \times 10^{-4} \text{ a.u.}$ due to the XUV electric-field strength which was set to unity in Ref. [26]. Finally, the spectrum in Fig. 3 of Ref. [26] was determined with a nonzero value for Δ_R . We find that we need to shift it by a value of -0.68 eV [Sec. VI] to achieve agreement. The structure in the figure is mostly due to the time dependence as the momentum dependence of the dipole and Auger decay matrix elements is weak. The differences between both curves are ascribed to a somewhat different treatment of the matrix elements.

We present the Auger electron spectrum for a dressing-laser intensity of $10^{13} \frac{\text{W}}{\text{cm}^2}$ in Fig. 7 [68]. The spectrum is first computed using generalized Bessel functions and a nonvanishing ponderomotive potential in Eq. (63). Then, it is determined using ordinary Bessel functions and $U_P = 0$. There are clear differences between the spectra. The convergence with respect to the number of terms in Eq. (40) is rapid; a summation from -2 to $+2$ in Eq. (40) was sufficient. We conclude that dressing-laser intensities around and above $10^{13} \frac{\text{W}}{\text{cm}^2}$ require an accurate treatment of the Volkov phase (41). We need 15 laser photon indices (Bessel functions) to account for absorption and emission of laser photons in the sum (61) for the Auger electron spectrum. This is in good agreement with previous studies of K -shell ionization of laser-dressed neon [22], argon [39], and krypton [38] atoms—however, with a very different theoretical approach—where 20, 12, and 5 photon blocks were required, respectively, to converge the calculations for the same dressing laser parameters that are used here. Seemingly crucial for the necessary number of photon blocks are the decay widths of the inner-shell hole which were 0.27 eV , 0.66 eV , and 2.7 eV ,

respectively. Our artificial value for the krypton $3d$ decay width of 1.3 eV lies between the decay widths of the krypton and the argon K shell vacancies.

VIII. CONCLUSION

We have devised and applied an *ab initio* theory for inner-shell XUV photoionization and subsequent Auger decay of laser-dressed atoms, a so-called two-color problem. Our work aims at the study and control of electron correlations—here manifested in terms of electronic decay—which is the most profound goal of attosecond science. The photo- and Auger electrons experienced an optical dressing laser which was considered to be intense but not strong enough to excite or ionize electrons in the atomic ground state. We used the Hartree-Fock-Slater (HFS) approximation as a starting point for the description of the atomic electronic structure. The HFS orbitals were then used to represent the full Hamiltonian. We employed a single configuration-state function to represent the ground state and singly- and doubly-excited states. The light fields were treated semi-classically and we use the strong-field approximation to treat the influence of the optical laser on the photo- and Auger electrons. The influence of the laser on the atomic ground-state electrons was neglected. The quantum dynamics of the problem was described in terms of equations of motion (EOMs). The EOMs were solved analytically for an essential-states model and a closed-form expression for the Auger electron amplitude was obtained. Furthermore, the XUV-absorption cross section of laser-dressed atoms and an expression for the laser-dressed photoelectron spectrum were derived. We applied our formalism to study the photoionization of

a $3d$ orbital (M shell) of a krypton atom and its subsequent $M_{4,5}N_1N_{2,3}$ Auger decay where the vacancy is filled with a $4s$ valence electron expelling a $4p$ valence electron. Following Ref. [26], we assumed an artificial decay width of krypton $3d$ vacancies of 1.3 eV. The atomic orbitals were approximated by suitably scaled hydrogen wave functions circumventing the need for a HFS computation. We discussed the approximations made and studied the convergence of the Auger decay matrix element and the expansion in terms of generalized Bessel functions. We compared our laser-dressed Auger spectrum to literature results of Smirnova *et al.* [26] and found good agreement. Finally, we presented the Auger electron spectrum for $10^{13} \frac{\text{W}}{\text{cm}^2}$ NIR laser intensity.

Our work opens up a multitude of future research perspectives. We have devised a general *ab initio* framework which allows us to create simplified models of varying sophistication tailored to model many physical situations in laser-dressed Auger decay. In this paper, we reduced our EOMs to an essential-states model which can be solved analytically and comprises sufficient details for a number of physical problems. In a forthcoming paper [40], we will use it to investigate coherence and interference of Auger electrons and their control by a laser. In a next step, our model can be generalized to a few states, e.g., all states in a subshell can be considered, avoiding magnetic quantum number-averaged dipole and Auger matrix elements.

Acknowledgments

We thank Olga Smirnova and Stephen H. Southworth for fruitful discussions. C.B. was supported by the National Science Foundation under Grant No. PHY-0701372.

-
- [1] P. Auger, *Compt. Rend. (Paris)* **177**, 169 (1923).
 - [2] D. Coster and R. Kronig, *Physica* **2**, 13 (1935).
 - [3] J. Als-Nielsen and D. McMorrow, *Elements of modern x-ray physics* (John Wiley & Sons, New York, 2001), ISBN 0-471-49858-0.
 - [4] A. C. Thompson, D. T. Attwood, E. M. Gullikson, M. R. Howells, J. B. Kortright, A. L. Robinson, J. H. Underwood, K.-J. Kim, J. Kirz, I. Lindau, et al., *X-ray data booklet* (Lawrence Berkeley National Laboratory, Berkeley, 2001), 2nd ed.
 - [5] H. P. Saha, *Phys. Rev. A* **42**, 6507 (1990).
 - [6] T. Åberg and G. Howat, in *Handbuch der Physik*, edited by W. Mehlhorn (Springer, Berlin, 1982), vol. 31, pp. 469–619, ISBN 3-540-11313-4.
 - [7] F. Gel'mukhanov and H. Ågren, *Phys. Rep.* **312**, 87 (1999).
 - [8] G. B. Armen, H. Aksela, H. Åberg, and S. Aksela, *J. Phys. B* **33**, R49 (2000).
 - [9] P. Agostini and L. F. DiMauro, *Rep. Prog. Phys.* **67**, 813 (2004).
 - [10] A. Scrinzi, M. Y. Ivanov, R. Kienberger, and D. M. Villeneuve, *J. Phys. B* **39**, R1 (2006).
 - [11] P. H. Bucksbaum, *Science* **317**, 766 (2007).
 - [12] H. Niikura and P. B. Corkum, *Adv. At. Mol. Opt. Phys.* **54**, 511 (2007).
 - [13] F. Krausz and M. Ivanov, *Rev. Mod. Phys.* **81**, 163 (2009).
 - [14] M. Drescher, M. Hentschel, R. Kienberger, M. Uiberacker, V. S. Yakovlev, A. Scrinzi, T. Westerwalbesloh, U. Kleineberg, U. Heinzmann, and F. Krausz, *Nature* **419**, 803 (2002).
 - [15] M. Drescher and F. Krausz, *J. Phys. B* **38**, S727 (2005).
 - [16] H. Aksela, S. Aksela, and H. Pulkkinen, *Phys. Rev. A* **30**, 2456 (1984).
 - [17] T. A. Carlson, D. R. Mullins, C. E. Beall, B. W. Yates, J. W. Taylor, D. W. Lindle, and F. A. Grimm, *Phys. Rev. A* **39**, 1170 (1989).
 - [18] M. Jurvansuu, A. Kivimäki, and S. Aksela, *Phys. Rev. A* **64**, 012502 (2001).
 - [19] B. Schmidtke, T. Khalil, M. Drescher, N. Müller, N. M. Kabachnik, and U. Heinzmann, *J. Phys. B* **34**, 4293 (2001).

- [20] P. Johnsson, J. Mauritsson, T. Remetter, A. L’Huillier, and K. J. Schafer, *Phys. Rev. Lett.* **99**, 233001 (2007).
- [21] J. Mauritsson, P. Johnsson, E. Mansten, M. Swoboda, T. Ruchon, A. L’Huillier, and K. J. Schafer, *Phys. Rev. Lett.* **100**, 073003 (2008).
- [22] C. Buth, R. Santra, and L. Young, *Phys. Rev. Lett.* **98**, 253001 (2007), arXiv:0705.3615.
- [23] S. N. Pisharody and R. R. Jones, *Science* **303**, 813 (2004).
- [24] S. X. Hu and L. A. Collins, *Phys. Rev. Lett.* **96**, 073004 (2006).
- [25] V. S. Yakovlev and A. Scrinzi (2002), supplement to Ref. [14]: www.nature.com/nature/journal/v419/n6909/supinfo/nature01488.html
- [26] O. Smirnova, V. S. Yakovlev, and A. Scrinzi, *Phys. Rev. Lett.* **91**, 253001 (2003).
- [27] V. S. Yakovlev, Dissertation, Technischen Universität Wien, Institut für Photonik, Gußhausstrasse 27/387, 1040 Wien, Austria (2003).
- [28] M. Kitzler, N. Milosevic, A. Scrinzi, F. Krausz, and T. Brabec, *Phys. Rev. Lett.* **88**, 173904 (2002).
- [29] M. V. Fedorov, *Atomic and free electrons in a strong light field* (World Scientific, Singapore, River Edge (New Jersey), 1997), ISBN 981-02-2902-X.
- [30] V. F. Weisskopf and E. P. Wigner, *Z. Phys.* **63**, 54 (1930).
- [31] J. J. Sakurai, *Modern quantum mechanics* (Addison-Wesley, Reading (Massachusetts), 1994), 2nd ed., ISBN 0-201-53929-2.
- [32] E. Merzbacher, *Quantum mechanics* (John Wiley & Sons, New York, 1998), 3rd ed., ISBN 0-471-88702-1.
- [33] Z. X. Zhao and C. D. Lin, *Phys. Rev. A* **71**, 060702(R) (2005).
- [34] M. Wickenhauser, J. Burgdörfer, F. Krausz, and M. Drescher, *Phys. Rev. Lett.* **94**, 023002 (2005).
- [35] A. K. Kazansky and N. M. Kabachnik, *Phys. Rev. A* **72**, 052714 (2005).
- [36] A. K. Kazansky and N. M. Kabachnik, *J. Phys. B* **40**, 2163 (2007).
- [37] O. Smirnova, V. S. Yakovlev, and M. Ivanov, *Phys. Rev. Lett.* **94**, 213001 (2005).
- [38] C. Buth and R. Santra, *Phys. Rev. A* **75**, 033412 (2007), arXiv:physics/0611122.
- [39] C. Buth and R. Santra, *Phys. Rev. A* **78**, 043409 (2008), arXiv:0809.3249.
- [40] C. Buth and K. J. Schafer, *J. Phys.: Conf. Ser.* pp. accepted, (2009), arXiv:0905.2647.
- [41] A. Szabo and N. S. Ostlund, *Modern quantum chemistry: Introduction to advanced electronic structure theory* (McGraw-Hill, New York, 1989), 1st, revised ed., ISBN 0-486-69186-1.
- [42] T. Åberg, *Phys. Scr.* **T41**, 71 (1992).
- [43] D. M. Wolkow, *Z. Phys.* **94**, 250 (1935).
- [44] L. B. Madsen, *Am. J. Phys.* **73**, 57 (2005).
- [45] R. Santra, C. Buth, E. R. Peterson, R. W. Dunford, E. P. Kanter, B. Krässig, S. H. Southworth, and L. Young, *J. Phys.: Conf. Ser.* **88**, 012052 (2007), arXiv:0712.2556.
- [46] C. Buth, R. Santra, and L. Young, *Rev. Mex. Fis. pp.* accepted, (2009), arXiv:0805.2619.
- [47] L. Young, C. Buth, R. W. Dunford, P. J. Ho, E. P. Kanter, B. Krässig, E. R. Peterson, N. Rohringer, R. Santra, and S. H. Southworth, *Rev. Mex. Fis. pp.* accepted, (2009), arXiv:0809.3537.
- [48] J. C. Slater, *Phys. Rev.* **81**, 385 (1951).
- [49] J. C. Slater and K. H. Johnson, *Phys. Rev. B* **5**, 844 (1972).
- [50] M. O. Scully and M. S. Zubairy, *Quantum optics* (Cambridge University Press, Cambridge, New York, Melbourne, 1997), ISBN 0-521-43595-1.
- [51] P. S. Epstein, *Phys. Rev.* **28**, 695 (1926).
- [52] R. K. Nesbet, *Proc. Roy. Soc. London* **A230**, 312 (1955).
- [53] C. Buth, R. Santra, and L. S. Cederbaum, *Phys. Rev. A* **69**, 032505 (2004), arXiv:physics/0401081.
- [54] We use the form of a Volkov wave [44] which is the solution of the time-independent Schrödinger equation for the interaction with the electric field in velocity form (33)—the interaction with the XUV light is in length form (9)—instead of the length form which is used in Ref. [26]. The difference of Eq. (4) in Ref. [26] to our Eq. (34) is the missing factor $e^{i\vec{A}_L(t)\cdot\vec{r}}$ in our expression [50].
- [55] H. R. Reiss, *Phys. Rev. A* **22**, 1786 (1980).
- [56] G. B. Arfken and H. J. Weber, *Mathematical methods for physicists* (Elsevier Academic Press, New York, 2005), sixth ed.
- [57] Our expressions are written for XUV light only; yet, in the corresponding expressions in Ref. [26], laser dressing is also considered. The slight deviations between both sets of equations due to these different situations are obvious and not mentioned here. Equation (10) in Ref. [26] differs from our Eq. (44) by a factor of $\frac{1}{\sqrt{2}}$ in the first term on the right-hand side and by a factor of $-2\sqrt{2}$ in the second term. Further, Eq. (11) in Ref. [26] agrees with our Eq. (45) apart from a factor of $\frac{-1}{\sqrt{2}}$.
- [58] C. Buth and R. Santra, *Phys. Rev. A* **77**, 013413 (2008), arXiv:0711.3203.
- [59] The difference between our expression (58)—in the limit of vanishing laser intensity—and Eq. (15) in Ref. [26] is a factor $\frac{-1}{\sqrt{2}}$ due to our more elaborate treatment of many-electron effects. Further the minus sign before Δ in Eq. (15) in Ref. [26] is a misprint. Smirnova *et al.* [26] found that their Eq. (15) without laser field is an excellent approximation for weak laser intensities to a numerically exact solution of the coupled differential equations with a laser field.
- [60] There is no additional factor of 2 in Eq. (68) compared with Eq. (31) in Ref. [38] to account for the number of electrons in a spatial orbital because our determinantal approach treats the transition from spin orbitals to spatial orbitals fully.
- [61] B. Talukdar, J. Dutta, and H. P. Chattopadhyay, *J. Phys. B* **17**, 3211 (1984).
- [62] M. E. Rose, *Elementary theory of angular momentum*, Structure of matter (John Wiley & Sons, New York, 1957), ISBN 0-486-68480-6.
- [63] J. D. Jackson, *Classical electrodynamics* (John Wiley & Sons, Chichester, New York, 1998), 3rd ed., ISBN 0-471-30932-X.
- [64] MATHEMATICA 7.0, Wolfram Research, Inc., Champaign, Illinois, USA (2008).
- [65] The energy of the krypton $3d$ shell of -96.6 eV which is used in Ref. [66] is lower than the value of -70 eV assumed for ε_{3d} in this paper. The photon energy needs to be adjusted accordingly to 116.6 eV to produce photoelectrons of the same kinetic energy in both cases.
- [66] J.-J. Yeh and I. Lindau, *At. Data Nucl. Data Tables* **32**, 1 (1985).
- [67] In the experiments on Auger decay of krypton $3d$ holes [14], the photoelectron was not observed and thus we integrate over its momentum [see Eq. (63)]. In

doing so, we neglect the impact of the laser on the photoelectrons. This is justified by considering Ref. [38], from which we know that the area under the cross section with and without laser dressing is approximately conserved. Hence, in our quite similar situation, we can assume that the integration over the photoelectron momentum does not vary noticeably whether the laser dressing of the photoelectrons is included or not.

[68] The Auger spectrum in Fig. 7 is very broad and extends down to ~ 25 eV. As the nominal photoelectron energy is 20 eV and the photoelectron spectrum is similarly broadened, the photo- and the Auger electron spectra overlap. To avoid this, a higher XUV photon energy may be used.